

**DYNAMIC ANALYSIS OF ADAPTIVE AIRCRAFT WINGS MODELLED AS
THIN-WALLED COMPOSITE BEAMS**

M.Sc. THESIS

Kaan YILDIZ

Department of Aeronautical and Astronautical Engineering

Aeronautical and Astronautical Engineering Programme

JANUARY 2015

**DYNAMIC ANALYSIS OF ADAPTIVE AIRCRAFT WINGS MODELLED AS
THIN-WALLED COMPOSITE BEAMS**

M.Sc. THESIS

**Kaan YILDIZ
(511131122)**

Department of Aeronautical and Astronautical Engineering

Aeronautical and Astronautical Engineering Programme

Thesis Advisor: Prof. Dr. Metin Orhan KAYA

JANUARY 2015

**İNCE CİDARLI KOMPOZİT KİRİŞ OLARAK MODELLENMİŞ
UYARLANABİLİR UÇAK KANATLARININ DİNAMİK ANALİZİ**

YÜKSEK LİSANS TEZİ

**Kaan YILDIZ
(511131122)**

Uçak ve Uzay Mühendisliği Anabilim Dalı

Uçak ve Uzay Mühendisliği Programı

Tez Danışmanı: Prof. Dr. Metin Orhan KAYA

OCAK 2015

Kaan YILDIZ, a M.Sc. student of ITU Graduate School of Science Engineering and Technology 511131122 successfully defended the thesis entitled “**DYNAMIC ANALYSIS OF ADAPTIVE AIRCRAFT WINGS MODELLED AS THIN-WALLED COMPOSITE BEAMS**”, which he prepared after fulfilling the requirements specified in the associated legislations, before the jury whose signatures are below.

Thesis Advisor : **Prof. Dr. Metin Orhan KAYA**
Istanbul Technical University

Jury Members : **Prof. Dr. Erol UZAL**
Istanbul University

Assist. Prof. Özge ÖZDEMİR
Istanbul Technical University

Date of Submission : **15 December 2014**

Date of Defense : **20 January 2015**

To my parents,

FOREWORD

I would like to express my sincere gratitude to my esteemed advisor Prof. Dr. Metin Orhan Kaya who gave me this tremendous opportunity to study as an advisee of his. I also appreciate him for always being there and backing me up in times of his guidance and experience are needed. I have learnt so much from him both in academic knowledge and life related issues.

Dr. Seher Eken is the other person that I can not possibly pay my debt to. She was literally always there, sharing her experience and knowledge without any hesitation, no matter what the subject is. I have never witnessed such a passion to study and self-improvement in anybody else and I feel very lucky to be inspired by her. Despite officially being a "mentor" to me, in my point of view, she is always considered as a friend to discuss any difficulties in my life.

I also wish to acknowledge the financial support of TÜBİTAK-BİDEB 2211.

Last but not least; I would like to thank my parents for their support and being there when I needed them to be. They supported and encouraged me all the time, and I wouldn't be who I am if it wasn't for them.

January 2015

Kaan YILDIZ
(Aeronautical Engineer)

TABLE OF CONTENTS

	<u>Page</u>
FOREWORD.....	ix
TABLE OF CONTENTS.....	xi
ABBREVIATIONS	xiii
LIST OF TABLES	xv
LIST OF FIGURES	xvii
SUMMARY	xix
ÖZET	xxi
1. INTRODUCTION	1
1.1 Literature Review	2
1.2 Purpose of Thesis	3
1.3 Overview	4
2. STRUCTURAL MODELLING AND FORMULATION	7
2.1 Thin Walled Composite Beam Theory	7
2.1.1 Displacement Field	8
2.1.1.1 In-plane displacements	8
2.1.1.2 Out-of plane displacements	9
2.1.2 Strain Field	11
2.1.3 Constitutive Equations.....	12
2.1.4 Energy Expressions	15
2.1.4.1 Strain energy	16
2.1.4.2 Kinetic energy.....	18
2.1.5 Equations of Motion	20
3. FREE VIBRATION.....	23
3.1 Structural Composite Configuration.....	23
3.2 Governing Equations of Motion	25
3.2.1 Extension-Twist Coupled Motion.....	25
3.2.2 Lateral Bending-Transverse Bending-Shear Coupled Motion	27
3.2.2.1 Shearable model.....	27
3.2.2.2 Unshearable model	28
3.3 Solution Methodology	29
3.4 Results and Discussion	31
4. ACTIVE VIBRATION CONTROL	37
4.1 Boundary Moment Control Law	39
4.2 Closed Loop Feedback Control Laws	40
4.2.1 Proportional Feedback Control Law.....	41
4.2.2 Velocity Feedback Control Law	42
4.3 Solution Methodology	42

4.4 Results and Discussion	45
4.4.1 Case Study-Timoshenko Beam.....	45
4.4.1.1 Symmetric case.....	47
4.4.1.2 Non-Symmetric case.....	49
4.4.2 Thin-walled Composite Beam.....	50
4.5 Optimal Feedback Control Law	56
4.6 Dynamic Response	58
5. CONCLUSION	65
REFERENCES.....	67
APPENDICES.....	69
APPENDIX A: Reduced Mass Terms and Stiffness Quantities.....	71
CURRICULUM VITAE.....	75

ABBREVIATIONS

CAS	: Circumferentially Asymmetric Stiffness
CUS	: Circumferentially Uniform Stiffness
DTI	: Direct Time Integration
DTM	: Differential Transform Method
EGM	: Extended Galerkin Method
LQR	: Linear Quadratic Regulator

LIST OF TABLES

	<u>Page</u>
Table 3.1 : Material Properties and Geometric Dimensions of The Box Beam....	32
Table 3.2 : Comparison of First Natural Frequencies for Box Beam.....	32
Table 4.1 : Material Properties and Geometric Dimensions of Timoshenko Beam	46
Table 4.2 : Comparison of First Natural Frequencies for Timoshenko Beam	48
Table 4.3 : Comparison of Second Natural Frequencies for Timoshenko Beam ..	48
Table 4.4 : Comparison of Third Natural Frequencies for Timoshenko Beam	49
Table 4.5 : Comparison of First Natural Frequencies for Timoshenko Beam	49
Table 4.6 : Comparison of Second Natural Frequencies for Timoshenko Beam ..	49
Table 4.7 : Comparison of Third Natural Frequencies for Timoshenko Beam	50
Table 4.8 : Material Properties of Piezoelectric Layers	50
Table A.1 : The reduced mass terms, b_i	71
Table A.2 : Stiffness quantities, $a_{ij} = a_{ji}$	72

LIST OF FIGURES

	<u>Page</u>
Figure 2.1 : Beam geometry before and after deformation.....	8
Figure 2.2 : Beam geometry and kinematic variables.....	9
Figure 2.3 : Stress resultants and stress couples	13
Figure 2.4 : N-layered composite beam	13
Figure 3.1 : CUS configuration	24
Figure 3.2 : Evaluation of the stiffness quantities, a_{ij}	26
Figure 3.3 : Variation of stiffness quantities versus ply angles	31
Figure 3.4 : First two natural frequencies of vertical bending mode of the box beam.....	33
Figure 3.5 : First two natural frequencies of lateral bending mode of the box beam.....	33
Figure 3.6 : The geometry of the diamond shaped thin walled beam	34
Figure 3.7 : Stiffness quantities for diamond shaped thin-walled beam	35
Figure 3.8 : First two natural frequencies of the diamond shaped thin-walled beam.....	35
Figure 4.1 : Timoshenko laminated beam.....	45
Figure 4.2 : (a) Symmetric laminate, (b) Non-symmetric laminate.....	46
Figure 4.3 : Variation of stiffness quantities with ply angle	50
Figure 4.4 : Variation of stiffness quantities with ply angle	51
Figure 4.5 : Natural frequencies of aircraft wing with diamond shaped cross section	52
Figure 4.6 : First natural frequencies versus K_p for selected ply angles, θ	53
Figure 4.7 : First natural frequencies versus K_p for selected values of length, L .	53
Figure 4.8 : First natural frequencies versus K_p for selected slenderness ratios, R	54
Figure 4.9 : First natural frequencies versus K_v for selected ply angles, θ	54
Figure 4.10 : First natural frequencies versus K_v for selected values of length, L ..	55
Figure 4.11 : First damping factors versus K_v for selected ply angles, θ	55
Figure 4.12 : Comparison of different control laws under applied Dirac Delta.....	60
Figure 4.13 : Comparison of different values of velocity feedback gains	61
Figure 4.14 : Dynamic response of the beam for optimal control under various control parameters.....	62
Figure 4.15 : Different damping characteristics.....	63

DYNAMIC ANALYSIS OF ADAPTIVE AIRCRAFT WINGS MODELLED AS THIN-WALLED COMPOSITE BEAMS

SUMMARY

There has been a growing interest in the development of the smart material systems technology due to their incorporation in various structures ranging from aeronautical/aerospace, automotive, helicopter and turbo-machinery rotor blades, robot manipulators. Using adaptive materials, the dynamical characteristics of the structure could be controlled in a predictable manner to avoid the dynamical instabilities such as structural resonances.

In this thesis, dynamic behaviour of aircraft wings is investigated and control of natural frequencies is achieved using piezoelectric actuation. Two different models namely, Timoshenko beam and thin-walled composite beam are used in this study. Natural frequencies of both model are obtained and using active control their variations are examined.

First, thin walled composite beam theory is introduced with detailed formulation including the effects of primary and secondary warping. This beam model also incorporates a number of non-classical effects such as material anisotropy, transverse shear deformation and warping restraint. Moreover, the directionality property of thin-walled composite beams produces a wide range of elastic couplings. In this respect, constitutive equations and energy expressions are given. Equations of motion are derived using Hamilton principle.

Second, in order to determine natural frequencies without piezoelectric influence, free vibration problem is formulated for an anti-symmetric lay-up configuration, also referred as Circumferentially Uniform Stiffness (CUS). Due to the anti-symmetry in lay-ups this configuration generates the coupled motion of transverse-lateral bending-shear. The equations of motion are discretized using Extended Glaerkin Method (EGM) to determine the natural frequencies of the system. The effect of transverse shear on the natural frequencies is also investigated by simply including and excluding transverse shear in the free vibration analyses, which has found to be significant for higher modes.

For validation purposes, analyses are conducted for a box beam thin walled composite beam and results are compared with the literature. Then, the analyses are repeated for a diamond shaped cross-section section and the results of different cross-sections are compared and discussed.

Active vibration control is introduced to gain an ability to control dynamic characteristics of structures. Implementation of piezoelectrically induced moments regarding the boundary moment is explained and two different control laws, namely proportional and velocity feedback control laws and their effects are investigated. The equations of motion that includes the effect of piezoelectric layers are cast into

the state-space representation to obtain the dynamic response of the beam. Before analyzing thin-walled composite beams, a numerical example is solved to attain a deeper understanding about the effect of piezoelectric materials on the natural frequencies. This beam model is developed using the first order shear deformable theory (Timoshenko beam theory) and then solved to determine the natural frequencies with and without piezoelectric layers influence for various boundary conditions and lay-ups.

Next, the similar analyses are also carried for thin walled composite beams highlighting the effects of piezoelectric layers, material anisotropy and transverse shear on the natural frequencies for varying feedback gains. Besides, several control laws such as proportional feedback gain and velocity feedback gain are used for vibration control and their results are compared. In addition, optimal control law is implemented and dynamic response of the structure is investigated using different control laws.

In conclusion, for a diamond shaped thin-walled composite aircraft wing, active vibration control is achieved using adaptive materials. Piezoelectric materials are used as sensors and actuators to provide closed-loop feedback control system. In future studies, response of the structure to the external forces will be investigated and controlled by using adaptive materials.

İNCE CİDARLI KOMPOZİT KİRİŞ OLARAK MODELLENMİŞ UYARLANABİLİR UÇAK KANATLARININ DİNAMİK ANALİZİ

ÖZET

Akıllı veya uyarlanabilir malzeme sistemleri teknolojilerinin geliştirilmesine gittikçe büyümekte olan bir ilgi gözlenmektedir. Bu ilginin en büyük sebebi bu tarz malzemelerin havacılık ve uzay, otomotiv, helikopter ve turbomakinelerin palleri ve robot kolları gibi çeşitli farklı yapılara kolayca uyarlanabilmesi ve kullanılabilir durumda olmasından kaynaklanmaktadır. Akıllı veya uyarlanabilir malzemelerin kullanımı ile, yapıların dinamik karakteristiklerinin öngörülebilir bir şekilde kontrol edilmesi mümkündür. Bu kontrol sayesinde yapısal rezonans ve çırpınma gibi bir takım dinamik kararsızlıkların önüne kolaylıkla geçilebilir.

Yapılmış olan bu tez çalışmasında, uçak kanatlarının dinamik davranışları incelenmiş ve piezoelektrik eyleyiciler yardımı ile doğal frekansların kontrolü sağlanmıştır. Bu tez boyunca iki farklı model kullanılmıştır. Bunlar sırasıyla Timoshenko kiriş ve ince cidarlı kompozit kiriş modelidir. Her iki model için de yapıların doğal frekansları hesaplanmış ve daha sonrasında akıllı malzemelerin yardımıyla doğal frekansların kontrolü sağlanarak, değişimleri incelenmiştir. Ayrıca yapının dinamik cevabı da farklı kontrol yasaları altında incelenmiştir.

İlk olarak, ince cidarlı kompozit kiriş teorisi tanıtılmıştır. Verilen formülasyon birincil ve ikincil çarpılma etkilerini içermektedir. Ayrıca bu kiriş modeli bir takım klasik olmayan etkileri de formülasyonunda barındırmaktadır. Bu klasik olmayan etkiler kısaca malzeme eşyönsüzlüğü, enlemesine kayma deformasyonu ve çarpılma kısıtlamasıdır. Diğer taraftan, ince cidarlı kompozit kirişlerin yönlülüğü, geniş bir elastik bağlaşım meydana getirmektedir. Bu bağlamda temel denklemler ve enerji ifadeleri verilmiştir. Daha sonrasında ise Hamilton Prensibi aracılığıyla genel hareket denklemlerinin eldesi gerçekleştirilmiştir.

Daha sonra serbest titreşim problemi açıklanmıştır. Bu problemi incelerken iki farklı kompozit konfigürasyonundan bahsedilmiş ve antisimetrik konfigürasyon, başka bir deyişle Circumferentially Uniform Stiffness (CUS) konfigürasyonu kullanılarak dikey-yatay eğilme ve enlemesine kayma bağlaşımli hareket denklemleri elde edilmiştir. Ayrıca, sırasıyla kayma etkilerini içeren ve içermeyen iki farklı teoriden bahsedilmiştir. Bu teoriler Shearable ve Unshearable Theory olarak literatürde bulunmaktadırlar. Serbest titreşim problemi hareket denklemlerine bir çözüm elde etmek için sayısal bir yöntem kullanılmıştır. Denklemlerin karmaşıklığı ve bağlaşımli olması analitik bir çözüm elde edilmesini imkansız kılmaktadır. Kullanılan sayısal yöntem Extended Galerkin Method olarak bilinmektedir ve bu kısımda açıklanmıştır. Bu metod, hareket denklemlerini ayırklaştırmakta ve bunu şekil fonksiyonları önererek gerçekleştirmektedir. İfadeler, şekil fonksiyonları ve genelleştirilmiş koordinatların çarpımı olarak tanımlanmaktadır. Bu yöntemin diğer sayısal yöntemlere göre üstünlüğü ise, önermiş olduğu şekil fonksiyonunun sadece geometrik sınır şartlarını

sağlamasının yeterliliğidir. Bu yöntemle hareket denklemleri çözülmüş ve doğal frekanslar elde edilmiştir.

Kanat elmas kesite sahip olacak şekilde modellenmeden önce oluşturulan matematik modelin doğruluğunu test etmek amacıyla referans kitaptan alınan sayısal bir örnek çözülmüştür. Çözülen bu örnek için elde edilen sonuçlar ve referans kitapta verilen sonuçlar karşılaştırılmıştır. Karşılaştırma sonucunda Extended Galerkin Metodu ile elde edilen sonuçlar ile kitap tarafından verilmiş olan sonuçların birbiriyle çok iyi bir uyum içerisinde olduğu görülmüştür. Böylece geliştirilmiş olan matematik modelin doğruluğu kanıtlanmıştır. Daha sonrasında kanat ince cidarlı kompozit kiriş olarak modellenmiştir. Serbest titreşim bölümünün sonucu olarak ise uçak kanatları için titreşim kontrolü yokluğunda doğal frekanslar elde edilmiştir.

Devamında aktif titreşim kontrolü konsepti, yapısal karakteristikler üzerinde bir kontrol sağlanması amacıyla sisteme eklenmiştir. Aktif kontrol tanımı verilmiş, piezoelektrik malzemeler tarafından indüklenen momentlerden bahsedilmiş ve sınır momenti hakkında detaylı bilgi verilmiştir. Ayrıca, uygulanmış olan iki farklı kontrol yasasından bahsedilmiştir. Bunlar sırasıyla orantısız geribesleme kontrol yasası ve hıza bağlı geribesleme yasası olarak adlandırılmaktadırlar. Aktif kontrolün sisteme katılması ile çözüm yönteminde modifikasyonlar yapılacağından durum uzay gösterimi anlatılmış ve sonuçlar elde edilmiştir.

Aktif geribesleme kontrolü uyarlanabilir malzemeler aracılığıyla sağlanmıştır. Piezoelektrik katmanlar ana yapının içerisine simetrik bir şekilde gömülmüş ve piezoelektrik eyleyiciler tüm kiriş uzunluğu boyunca yayılmıştır. Bunun sonucu olarak, kirişin uç noktasında bir sınır momenti indüklenmiş ve bunlar hareket denklemlerini etkilemek yerine sınır şartlarında tekil moment ifadeleri olarak yer almışlardır. Orantısız ve hıza bağlı geribesleme kontrol yöntemleri kullanılmış ve elyaf açısı dağılımının temel frekanslar üzerindeki etkisi incelenmiştir. Doğal frekanslar elde edilirken kütle ve katılık matrislerine piezoelektrik katmanların etkisi de eklenmiştir. Bu etkinin ihmal edildiği durum için de analizler yapılmış ve sonuçlar karşılaştırıldığında doğal frekanslarda yaklaşık olarak %5'lik bir fark ortaya çıkmıştır. Literatürdeki çoğu çalışmada bu etkiler ihmal edilirken, yapılan bu tez çalışmasında bu etkinin önemine de vurgu yapılmıştır.

Son olarak, piezoelektrik etkileri iyice algılamak ve anlamak amacıyla Timoshenko kiriş teorisini içeren bir örnek çalışma göz önüne alınmış ve orantısız geribesleme kontrol yasası uygulanarak doğal frekanslar bu örnek kiriş için elde edilmişlerdir. Bu örneğin hareket denklemleri ince cidarlı kiriş modelindeki denklemler kadar zor olmadığından analitik bir çözüm elde etmek mümkün olmuştur. Analitik yöntemin yanı sıra, problem yarı-analitik yöntem olan Differential Transform Method (DTM) ve Extended Galerkin Method (EGM) ile tekrar çözülmüştür. Elde edilen sonuçlar ilgili yerlerde tablo halinde verilmiştir. Bir sonraki adımda ise, uçak kanadımız artık elmas kesitli ince cidarlı kiriş olarak ele alınarak üzerine kontrol yasaları uygulanmıştır. Değişen kontrol kazançları ile doğal frekanslar elde edilmiş ve grafik olarak gösterilmişlerdir. Daha sonra modeli daha iyi analiz etmek amacıyla uzunluk ve narinlik oranı gibi parametreler değiştirilerek doğal frekansların incelendiği çalışma yapılmıştır, sonuçlar grafik üzerinde gösterilmişlerdir. Optimal kontrol yasası tanıtılmış ve yapıya uygulanması gerçekleştirilmiştir. Ayrıca, kiriş ucuna uygulanan Dirac Delta impulsu altında yapının dinamik cevabı incelenmiş, çeşitli kontrol yasaları için karşılaştırma yapılmıştır.

Sonuç olarak, elmas şeklinde ara kesite sahip olan ince cidarlı kompozit uçak kanadı için, aktif titreşim kontrolü akıllı malzemeler aracılığıyla sağlanmıştır. Piezoelektrik malzemeler kapalı devre geribesleme kontrol sistemini sağlamak amacıyla algılayıcı ve eyleyici olarak kullanılmışlardır. Gelecek çalışmalarda ise yapının dışarıdan gelecek olan kuvvetlere vereceği cevabın incelenmesi ve kontrolünün sağlanması gerçekleştirilecektir.

1. INTRODUCTION

Thin walled composite beams are being used widely in many advanced fields ranging from aerospace to mechanical, civil and naval constructions. The growing interest of thin walled structures arise from their incorporation in these fields in order to bring new designs to perfection, making them efficient, able to operate in extreme environmental conditions [1].

Thin walled composite beam theory involves with a wide range of elastic couplings due to its directionality property. In this respect, considering each possible case, it is likely to analyze the dynamic behaviours of the structures and especially, instabilities can be avoided. Moreover, this theory incorporates a number of non-classical effects such as material anisotropy, transverse shear deformation and warping restraint which enables modelling much more accurately.

Practice of adaptive materials into structures is one of the most attracting subjects in past decades. Utilization of these materials has expanded the use and capabilities of thin walled structures. It became possible to meet the demanding requirements of complex environments, with the contribution of adaptive materials. Static and dynamic response, stability and control of structures have been enhanced with adaptive material technology.

In this study, the closed-loop vibrational behaviour of aircraft wing is investigated. The wing is modelled as a thin-walled composite beam with a diamond shaped cross-section. In order to inspect relevant coupling case, an anti-symmetric lay-up configuration i.e. Circumferentially Uniform Stiffness (CUS) is employed and coupled motion of transverse-lateral bending and transverse shear is generated. The active feedback control is performed by using piezoelectric ceramics as adaptive materials. The piezoelectric layers are symmetrically embedded in the host structure and the piezoactuator is spread over the entire beam span. As a result of this, a boundary moment is induced at the beam tip and in this case, the control is achieved via the boundary moment feedback control yielding an adaptive change in the dynamical

characteristics of the beam. The cases of proportional and velocity feedback control procedures are applied and the effect of ply-angle orientation on the fundamental frequencies are investigated and discussed.

1.1 Literature Review

From a historical perspective, the assumption of thin-walled beams came into being in late 1930s. After the World war II, strong studies were made on the theory, and many books were published related to the issue such as Librescu and Ohseop's monograph named "Thin-walled composite beams: Theory and Application", [1]. Also, some studies are made on linear static and dynamic behaviour of thin-walled composite beams of closed cross-section such as the study of "Theory of anisotropic thin-walled closed-cross-section beams" presented by Berdichevsky, Armanios and Badir [2]. In last two decades, many studies are made to develop the thin walled composite beam theory and enlarging its area of integration in various structures such as aeronautical/aerospace vehicles, automobiles, helicopter and turbo machinery rotor blades and other mechanical, civil to naval constructions. The behaviour of two non-classical impacts namely elastic bending-shear coupling and restrained torsional warping in the behaviour of thin walled composite beams is researched in Rehfield's work, intimately [3]. Also, in purpose of isolating the impact of coupling on the free vibration of closed section beams under extension-twist or bending-twist coupling using the assumption that is revised by Armanios and Badir, Danicilia made her research named "The influence of coupling on the free vibration of anisotropic thin-walled closed-section beams" [4].

Despite the aircraft wing is modeled as a beam with solid cross-section commonly in the literature, there are only few researches are made to investigate the dynamic analysis of thin-walled composite beams. Uniquely, Librescu's work "Free Vibration of Anisotropic Composite Thin-walled Beams of Closed Cross-Section Contour" led the approach of the dynamic behaviour of thin-walled composite beams [5]. In his work mentioned, the impact of directionality property of advanced composite materials and non-classical impacts are introduced. In another study, Librescu investigated the dynamic aeroelastic response and the related robust control of aircraft swept wings, subjugated to gust of wind and fulminating type loads.

Regarding control concept of the structures, use of piezoelectric actuators firstly introduced by Bailey and Hubbard (1985). The actuators are located at outer surface of the beam and their mechanical models are developed by Crawley and Luis (1987). New theories concerning embedded piezoactuators and sensors are developed by Lee (1990), Wang and Rogers (1991), Batra and Ghosh (1995) and Mitchell and Reddy (1995). Tzou used piezoelectric shells and generated boundary moment to obtain control ability on structures (1993) [6]. Active control are applied to thin walled composite beams by Librescu and his colleagues [1, 7–9] in late 1990s.

There are many studies in active vibration control of structures using adaptive materials, especially piezoelectric in last decade. Their implementation to the thin walled aircraft structures offers great improvements in design efficiency. Librescu has taken the role of a pioneer in this field [10–12]. Also, advanced control systems such as optimal control, are implemented in structures [13] and new aircraft wing geometries are being investigated [14].

1.2 Purpose of Thesis

The dynamic behaviour of a thin walled beam with diamond cross section is investigated. It is aimed to control the dynamic behaviour of the aircraft wing so that any instabilities can be avoided. Active vibration control of the aircraft wing is achieved by adaptive materials and variation of the natural frequencies versus control gain is examined.

Firstly, the aircraft wing is modelled as a diamond shaped thin walled composite beam. An anti-symmetric composite lay-up, also known as Circumferentially Uniform Stiffness Configuration, is used and transverse bending-lateral bending-shear coupled motion is generated and investigated. The governing equations of motion are derived using Hamilton's principle and solution is obtained numerically by Extended Galerkin Method. Validation of the solution and mathematical model is accomplished by a numerical example from Ref. [1].

Secondly, as mentioned, in order to prevent dynamical instabilities such as resonance or flutter, active vibration control as a closed loop control system is implemented into the structure. Prior to introduction of active control into thin walled composite beams,

it is tested on a Timoshenko beam and variation of natural frequencies is determined versus proportional feedback gain. Afterwards, two different control laws are used to control the natural frequencies of the thin walled structure and as a result in a predictable manner it is achieved. Proportional feedback control law has no big impact on natural frequencies while velocity feedback law shows much better control ability. In the absence of velocity feedback law, no damping is obtained as expected. On the other hand, when velocity feedback law is implemented, damping is acquired as an output.

In conclusion, for thin walled composite beams, the model is validated by solving a numerical example. Then, as main focus, the aircraft wing is modelled as a thin walled beam and natural frequencies are obtained. Afterwards, in order to obtain a good knowledge on how active vibration control works, a Timoshenko piezo-laminated beam has been taken into consideration and variation of natural frequencies is calculated. Lastly, active vibration is applied to diamond shaped thin walled aircraft wing and natural frequencies, their variations, damping ratios and dynamic response of the beam are obtained.

1.3 Overview

This section is devoted to provide a detailed information to reader, about what each chapter is interested in. Readers who would like to earn a comprehensive knowledge about thin walled structures and active vibration control, should refer to each chapter one by one.

Chapter 2 deals with structural modelling of the thin walled composite beams. Kinematic assumptions and variables are mentioned firstly. Then detailed expressions and formulation of displacement and strain field are given. Also details of constitutive equations and energy expressions are pointed out. Using energy expressions and utilizing Hamilton's principle, the equations of motion are derived. All derivations and formulations on this chapter are based on linear theory.

Chapter 3 defines the free vibration problem and underlines its importance. Two different structural composite configurations are mentioned here and the one, Circumferentially Uniform Stiffness Configuration, which is employed in this study,

is investigated broadly. Equations of motion are rearranged for the coupling which the structural composite configuration involves. Determination of stiffness quantities are mentioned and a chart is provided for it. Shearable and unshearable model are given and solution methodology is examined. Solution of the equations for free vibration problem gives the natural frequencies and validation is acquired. Eventually in this chapter, the results are provided for a diamond shaped beam.

In Chapter 4, one can learn the concept of active vibration control, how it is implemented into structures using adaptive materials. Modified equations of motion due to piezoelectric actuation are derived. Boundary moment control law is introduced and two different closed loop feedback control laws are explained and their equations are provided. Due to active vibration, solution methodology differs a little bit and state space representation is used. Then a case study is taken into account, piezo-laminated Timoshenko beam. Its equations of motion are given and solutions are obtained analytically and numerically. Afterwards, thin walled aircraft wing is considered again and natural frequencies are obtained as well as their variations and damping factors. Additionally, implementation of optimal control law is achieved and dynamic response of the beam is investigated.

Chapter 5 concludes the whole study briefly. Besides it mentions about how study will be extended and continued.

2. STRUCTURAL MODELLING AND FORMULATION

This chapter focuses on thin walled composite beam theory, formulation and its applications. The theory which is quite complicated and can be thought as combination of bar and shell structures, considerably differs from other beam theories due to its non-classical effects. These non-classical effects can be listed as material anisotropy, transverse shear deformation and warping restraint. In order to model thin walled structures such as aircraft wings, ship hulls, pipes, culvert and box girder bridges, in a precise and accurate way, thin walled composite beam theory offers a great opportunity. The implementation of that theory promises great results compatible with experimental results. In the following subsequent subsections, formulation and structural modelling of the theory are given in a detailed way.

2.1 Thin Walled Composite Beam Theory

Continuous development of technology has created new opportunities for humans to improve their designs and aspects of engineering. The foremost new design idea for structural mechanics is using high strength to density structures. This can be achieved by either adapting new materials like composites or changing the shape of the geometry to hollow type closed sections. Both changing the geometry and adapting composites into the structures lead to thin walled composite beam theory.

This most challenging and modern field of structural mechanics was firstly introduced by Librescu and Song. The formulation of modern linear theory of thin-walled composite beams provides powerful mathematical tool to make related calculations and is investigated in next subsections. There are some kinematic assumptions made and the most important ones are listed below.

1. The shape of the cross-section does not deform in its own plane.
2. The rate of twist ϕ' varies along x-coordinate(spanwise). This assumptions yields a non-uniform torsional model which is also referred as the restrained-torsion model.

3. The material properties vary in both circumferential and normal direction (anisotropy).
4. A static statement also implies that the circumferential stress resultant N_{ss} , which is known as hoop stress is negligibly small.

2.1.1 Displacement Field

In this section the formulation of displacement field which consists of in plane and out-of plane displacements, is derived. Here, a cantilever beam is considered and its geometry before and after deformation can be seen in Figure 2.1. Beam has a length L , characteristic length d and wall thickness h . S point, located at mid-contour, moves to S' with translations of u, v, w and rotation of ϕ .

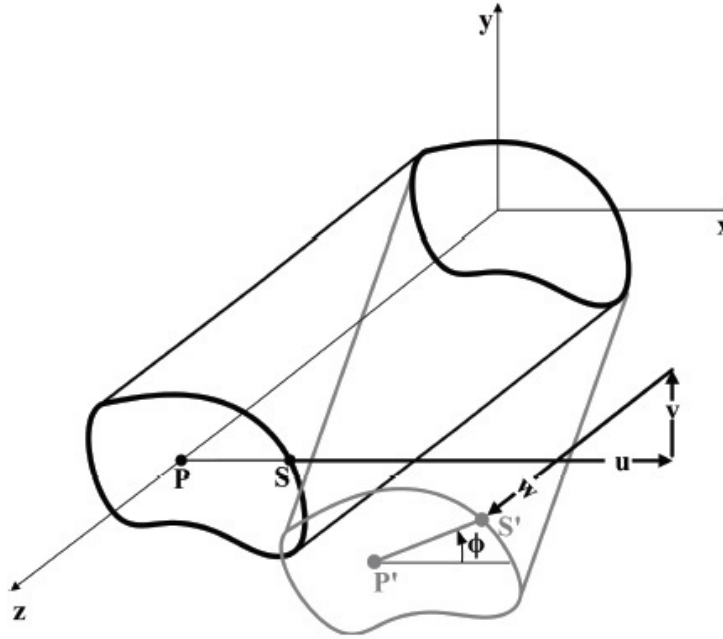


Figure 2.1: Beam geometry before and after deformation

The expressions of these translations and rotation is given separately in the following subsections.

2.1.1.1 In-plane displacements

Considering the beam as two-dimensional and focusing on cross section helps us to obtain expressions for in-plane translations. The two dimensional figure of the cross section before and after deformation can be seen in Figure 2.2.

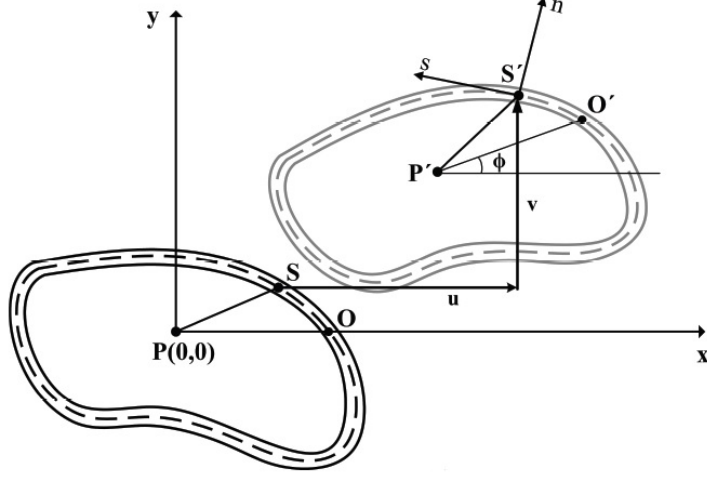


Figure 2.2: Beam geometry and kinematic variables

The in-plane translations of point $S(x, y)$ at mid-contour are given as:

$$u(x, y, z, t) = u_0(z, t) - y\phi(z, t) \quad (2.1)$$

$$v(x, y, z, t) = v_0(z, t) + x\phi(z, t) \quad (2.2)$$

Here t denotes time while u_0 and v_0 denote displacements of pole point P . Also rotation of the cross-section is represented with the symbol of $\phi(z, t)$. The detailed derivation of these expressions can be found in Ref. [1, 15].

2.1.1.2 Out-of plane displacements

Out-of plane displacement expression varies for open and closed cross-sections. The difference between them originates from torsional shear strain expressions. Since our interest lays in the aircraft wings, open cross-section beams are not investigated in this thesis.

For a closed cross-section beams the torsional shear strain corresponds a constant shear flow with respect to tangential axis. The direct shear strain for a single-cell closed cross-section beam is given as Ref. [1, 8].

$$\gamma_{sz} = -\frac{dx}{ds}\gamma_{xz} + \frac{dy}{ds}\gamma_{yz} + 2n\phi' \quad (2.3)$$

For closed cross-section beam, Vlasov's assumption for the shear strain is given as

$$\gamma_{sz} = \frac{\partial u_t}{\partial z} + \frac{\partial w}{\partial s} \quad (2.4)$$

Considering these two shear strain expression yields

$$\frac{\partial w}{\partial s} = \theta_x(z, t) \frac{dy}{ds} + \theta_y(z, t) \frac{dx}{ds} - r_n(s) \phi'(z, t) \quad (2.5)$$

Here, θ_x and θ_y represents the rotation about x and y axes respectively, defined as

$$\theta_x(z, t) = \gamma_{yz} - v'_0 \quad (2.6)$$

$$\theta_y(z, t) = \gamma_{xz} - u'_0 \quad (2.7)$$

The axial displacement expression for mid-surface ($n = 0$) can be obtained by integrating Eq. 2.5

$$w(s, z, t) = w_0(z, t) + y(s) \theta_x(z, t) + x(s) \theta_y(z, t) - F_w(s) \phi'(z, t) \quad (2.8)$$

This expression is valid for both open and closed cross-section beams. The function F_w in Eq. 2.8 is known as primary warping function. Secondary warping is related to contributions of the points off the mid-surface and needs to be taken into account when considering thick-walled beams. Eventually, Eq.2.9 defines the axial displacement with contributions from both primary and secondary warping effects.

$$w(s, z, t) = w_0(z, t) + \left[y(s) - n \frac{dy}{ds} \right] \theta_x(z, t) + \left[x(s) + n \frac{dx}{ds} \right] \theta_y(z, t) - \left[F_w(s) - n r_t(s) \right] \phi'(z, t) \quad (2.9)$$

Here, expression of the primary warping function is given as

$$F_w = \oint_C [r_n(s) - \psi(s)] ds \quad (2.10)$$

The other terms in Eq. 2.9 with n multipliers in front of them are related to secondary warping and importance of them increases while dealing with thick-walled beams.

2.1.2 Strain Field

Strain field is expressed with the similar common small displacements assumption equations

$$\epsilon_{xx} = \frac{\partial u}{\partial x}; \quad \epsilon_{yy} = \frac{\partial v}{\partial y}; \quad \epsilon_{zz} = \frac{\partial w}{\partial z}; \quad (2.11)$$

$$\gamma_{xy} = \frac{1}{2} \left(\frac{\partial u}{\partial y} + \frac{\partial v}{\partial x} \right); \quad \gamma_{yz} = \frac{1}{2} \left(\frac{\partial v}{\partial z} + \frac{\partial w}{\partial y} \right); \quad \gamma_{xz} = \frac{1}{2} \left(\frac{\partial u}{\partial z} + \frac{\partial w}{\partial x} \right) \quad (2.12)$$

Regarding the first assumption, the cross-sections do not deform in its own plane, obtained translation equations are substituted into strain field equations, Eq. 2.11 and 2.12 yields

$$\epsilon_{xx} = 0; \quad \epsilon_{yy} = 0; \quad \gamma_{xy} = 0; \quad (2.13)$$

which means that the first assumption holds. Furthermore, the non-zero strain components can be arranged as below using newly obtained translation expressions

$$\epsilon_{zz}(s, z, n, t) = \epsilon_{zz}^{(0)}(s, z, n, t) + n\epsilon_{zz}^{(1)}(s, z, t) \quad (2.14)$$

where

$$\begin{aligned} \epsilon_{zz}^{(0)}(s, z, n, t) = & w'_0(z, t) + y(s)\theta'_x(z, t) + x(s)\theta'_y(z, t) \\ & - \phi''(z, t) \left[\int_0^s r_n(\lambda) d\lambda - \int_0^s \frac{r_n(s) ds}{\oint ds} d\lambda \right] \end{aligned} \quad (2.15)$$

and

$$\epsilon_{zz}^{(1)}(s, z, t) = \frac{dy}{ds}\theta'_y(z, t) - \frac{dx}{ds}\theta'_x(z, t) - \phi''(z, t)r_t(s) \quad (2.16)$$

Furthermore, the shear strain components off the mid-line contour can be expressed in terms of displacements

$$\Gamma_{sz}(s, z, n, t) = \gamma_{sz}^{(0)}(s, z, n, t) + \gamma_{sz}^{(t)}(s, z, n, t) + n\gamma_{sz}^{(1)}(s, z, t) \quad (2.17)$$

$$\Gamma_{nz}(s, z, n, t) = \gamma_{nz}^{(0)}(s, z, n, t) \quad (2.18)$$

where

$$\gamma_{sz}^{(0)}(s, z, n, t) = \frac{dx}{ds} [u'_0(z, t) + \theta_y(z, t)] + \frac{dy}{ds} [v'_0(z, t) + \theta_x(z, t)] \quad (2.19)$$

$$\gamma_{sz}^{(t)}(s, z, t) = \psi(s)\phi'(z, t) \quad \text{where} \quad \psi(s) = \frac{\oint r_n(s) ds}{\oint ds} \quad (2.20)$$

$$\gamma_{sz}^{(1)}(s, z, t) = 2\phi'(z, t) \quad (2.21)$$

and

$$\gamma_{nz}^{(0)}(s, z, n, t) = \frac{dy}{ds} [u'_0(z, t) + \theta_y(z, t)] - \frac{dx}{ds} [v'_0(z, t) + \theta_x(z, t)] \quad (2.22)$$

The superscript $(.)^{(0)}$ denotes the strain components which has a numerical value different from zero at mid-line contour only while $(.)^{(1)}$ denoting the strains which are different from zero off the mid-line contour.

2.1.3 Constitutive Equations

The i^{th} layer's constitutive equations of an N layered thin-walled composite beam are given as

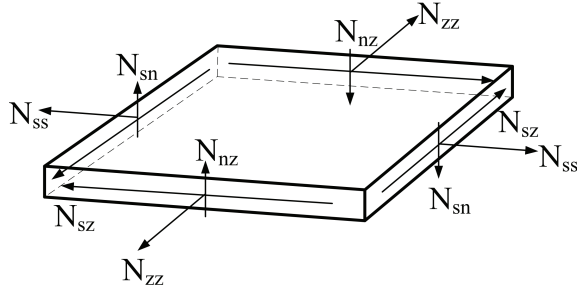
$$\begin{Bmatrix} \sigma_{ss} \\ \sigma_{zz} \\ \sigma_{zn} \\ \sigma_{sn} \\ \sigma_{sz} \end{Bmatrix}_{(i)} = [Q]_{(i)} \begin{Bmatrix} \epsilon_{ss} \\ \epsilon_{zz} \\ \epsilon_{zn} \\ \epsilon_{sn} \\ \epsilon_{sz} \end{Bmatrix}_{(i)} \quad (2.23)$$

Here, $[Q]$ is known as the reduced stiffness matrix.

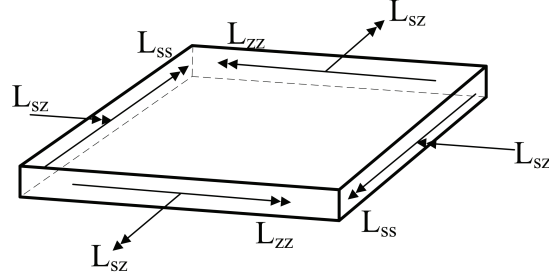
The membrane stress resultants N_{ss} , N_{zz} , N_{sz} ; the transverse shear resultants N_{ss} , N_{ss} and the stress couples N_{ss} , N_{ss} , N_{ss} are shown on a beam element in Figure 2.3.

In Figure 2.4, geometry of an N layered thin-walled composite beam is seen. Both Cartesian (x, y, z) and curvilinear (s, n, z) coordinates are apparent on the figure.

The stress resultants symbolize forces while the stress couples stand for moments. The stress resultants have the unit force per unit length and the stress couples have the unit of moment per unit length. Their expressions are given below



(a) Stress Resultants



(b) Stress Couples

Figure 2.3: (a) Stress resultants, (b) stress couples

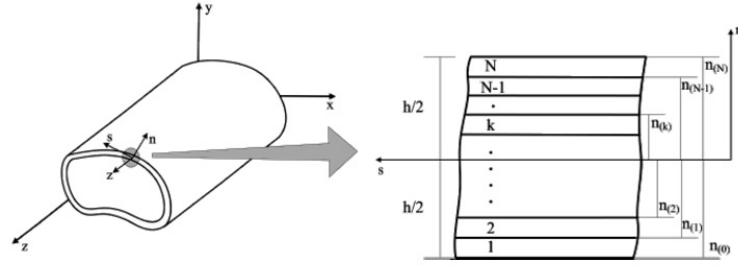


Figure 2.4: N-layered composite beam

- The stress resultants

$$\begin{Bmatrix} N_{ss} \\ N_{zz} \\ N_{sz} \\ N_{zn} \\ N_{sn} \end{Bmatrix} = \sum_{i=1}^N \int_{n_{(i-1)}}^{n_{(i)}} \begin{Bmatrix} \sigma_{ss} \\ \sigma_{zz} \\ \sigma_{sz} \\ \sigma_{zn} \\ \sigma_{sn} \end{Bmatrix}_{(i)} dn \quad (2.24)$$

- The stress couples

$$\begin{Bmatrix} L_{zz} \\ L_{sz} \end{Bmatrix} = \sum_{i=1}^N \int_{n_{(i-1)}}^{n_{(i)}} \begin{Bmatrix} \sigma_{zz} \\ \sigma_{sz} \end{Bmatrix}_{(i)} n dn \quad (2.25)$$

The thickness and tangential shear stiffness of the layered composite beam are assumed to be uniform along the tangential axis, s , constitutive equations for closed cross-section beams are expressed as

$$\begin{Bmatrix} N_{ss} \\ N_{zz} \\ N_{sz} \end{Bmatrix} = \begin{bmatrix} A_{11} & A_{12} & A_{16} \\ A_{12} & A_{22} & A_{26} \\ A_{16} & A_{26} & A_{66} \end{bmatrix} \begin{Bmatrix} \epsilon_{ss} \\ \epsilon_{zz}^{(0)} \\ \gamma_{sz}^{(0)} + \gamma_{sz}^{(t)} \end{Bmatrix} + \begin{Bmatrix} B_{12} \\ B_{22} \\ B_{26} \end{Bmatrix} \epsilon_{zz}^{(1)} + \begin{Bmatrix} B_{16} \\ B_{26} \\ B_{66} \end{Bmatrix} \gamma_{sz}^{(1)} \quad (2.26)$$

$$N_{zn} = A_{44} \gamma_{zn} \quad (2.27)$$

$$N_{sn} = A_{45} \gamma_{zn} \quad (2.28)$$

$$\begin{Bmatrix} L_{zz} \\ L_{sz} \end{Bmatrix} = \begin{bmatrix} B_{12} & B_{22} & B_{26} \\ B_{16} & B_{26} & B_{66} \end{bmatrix} \begin{Bmatrix} \epsilon_{ss} \\ \epsilon_{zz}^{(0)} \\ \gamma_{sz}^{(0)} + \gamma_{sz}^{(t)} \end{Bmatrix} + \begin{Bmatrix} D_{22} \\ D_{26} \end{Bmatrix} \epsilon_{zz}^{(1)} + \begin{Bmatrix} D_{26} \\ D_{66} \end{Bmatrix} \gamma_{sz}^{(1)} \quad (2.29)$$

The constitutive equations contain some stiffness quantities known from classical laminate theory and they are expressed in Ref. [16] as

$$A_{jk} = \sum_{i=1}^N \int_{n_{(i-1)}}^{n_{(i)}} Q_{jk}^{(i)} dn \quad (2.30)$$

$$B_{jk} = \sum_{i=1}^N \int_{n_{(i-1)}}^{n_{(i)}} Q_{jk}^{(i)} n dn \quad (2.31)$$

$$D_{jk} = \sum_{i=1}^N \int_{n_{(i-1)}}^{n_{(i)}} Q_{jk}^{(i)} n^2 dn \quad (2.32)$$

Here, these stiffness quantity terms are called extensional stiffness, coupling stiffness and bending stiffness respectively.

The transverse shear stiffness quantities are also given as

$$A_{lm} = \sum_{i=1}^N \int_{n_{(i-1)}}^{n_{(i)}} k_{lm}^2 Q_{jk}^{(i)} dn \quad (2.33)$$

In this expression, Reissner's transverse shear correction factor is used. $k_{lm} = \sqrt{5/6}$

Fourth kinematic assumption involves here with the constitutive equations. The circumferential stress resultant N_{ss} , which is known as hoop stress is negligible compared to other stresses and becomes zero. By this assumption, tangential strain becomes

$$\epsilon_{ss} = -\frac{1}{A_{11}} \left(A_{12} \epsilon_{zz}^{(0)} + A_{16} \gamma_{sz}^{(0)} + A_{16} \gamma_{sz}^{(t)} + B_{16} \gamma_{sz}^{(1)} + B_{12} \epsilon_{zz}^{(1)} \right) \quad (2.34)$$

Eventually, constitutive equations for single cell closed thin-walled beams are obtained as below

$$\begin{Bmatrix} N_{zz} \\ N_{sz} \\ L_{zz} \\ L_{sz} \\ N_{zn} \\ N_{sn} \end{Bmatrix} = \begin{bmatrix} K_{11} & K_{12} & K_{13} & K_{14} & 0 \\ K_{21} & K_{22} & K_{23} & K_{24} & 0 \\ K_{41} & K_{42} & K_{43} & K_{44} & 0 \\ K_{51} & K_{52} & K_{53} & K_{54} & 0 \\ 0 & 0 & 0 & 0 & A_{44} \\ 0 & 0 & 0 & 0 & A_{45} \end{bmatrix} \begin{Bmatrix} \varepsilon_{zz}^{(0)} \\ \gamma_{sz}^{(0)} \\ \gamma_{sz}^{(1)}/2 \\ \varepsilon_{zz}^{(1)} \\ \gamma_{nz}^{(0)} \end{Bmatrix} \quad (2.35)$$

2.1.4 Energy Expressions

In order to derive the equations of motion for thin-walled composite beams, Hamilton's principle is utilized. Hamilton's principle requires strain energy and kinetic energy expressions as well as work done by external forces to obtain equations of motion. U , K and W_e represent strain or potential energy, kinetic energy and work done by external forces, respectively. The displacements denoted by $\Delta_i = \Delta_i(x, y, z, t)$ satisfy the boundary conditions $\Delta_i = \bar{\Delta}_i$ and the variations of the displacements also fulfill the condition $\delta\Delta_i = 0$ at two arbitrary times, t_0 and t_1 . Hamilton's principle ensures that the following expression which is also called as variational, is constant for the motion's original path from time t_0 to t_1 and given as

$$\delta J = \int_{t_0}^{t_1} \delta(U - K - W_e) dt = 0 \quad (2.36)$$

where J and δ are Hamilton function and variation operator, respectively. The strain and kinetic energy expressions are respectively

$$U = \frac{1}{2} \int_V \sigma_{ij} \varepsilon_{ij} dV \quad (2.37)$$

$$K = \frac{1}{2} \int_V \rho \dot{\Delta}_i \dot{\Delta}_i dV \quad (2.38)$$

To handle the kinetic energy in the variational formulation,

$$\begin{aligned} \int_{t_0}^{t_1} \delta K dt &= \int_{t_0}^{t_1} \rho \dot{\Delta}_i \delta \dot{\Delta}_i dt \\ &= \rho \dot{\Delta}_i \delta \Delta_i \Big|_{t=t_0}^{t_1} - \int_{t_0}^{t_1} \rho \ddot{\Delta}_i \delta \Delta_i dt \end{aligned} \quad (2.39)$$

Here, $(\dot{\cdot})$ presents the partial derivative with respect to time t . Hamilton principle stipulates that $\delta\Delta_i(x, y, z, t_0) = \delta\Delta_i(x, y, z, t_1) = 0$ yielding the first term on the right hand side of Eq. 2.44 is removed thereby updating the expression of δJ

$$\delta J = \int_{t_0}^{t_1} \delta(U + \bar{K} - W_e) dt = 0 \quad (2.40)$$

where $\delta\bar{K} = -\rho\ddot{\Delta}_i\delta\Delta_i$.

2.1.4.1 Strain energy

The strain energy per unit volume can be expressed as multiplication of stress and strain. In order to obtain total strain energy of the beam, the strain energy per unit volume should be integrated all over the volume. Since ϵ_{xx} , ϵ_{yy} and γ_{xy} are assumed and found as zero, the strain energy is calculated with non-zero strain components as

$$U = \frac{1}{2} \int_0^L \oint_C \int_h [\sigma_{zz}\epsilon_{zz} + \sigma_{sz}\Gamma_{sz} + \sigma_{nz}\Gamma_{nz}]_{(i)} dndsdz \quad (2.41)$$

The integration through the wall thickness is carried out and using stress resultant and stress couple expressions, the strain energy can be re-expressed as

$$\begin{aligned} U &= \frac{1}{2} \int_0^L \oint_C \int_h \left\{ \sigma_{zz} [\epsilon_{zz}^{(0)} + n\epsilon_{zz}^{(1)}] \right. \\ &\quad \left. + \sigma_{sz} [\gamma_{sz}^{(0)} + \gamma_{sz}^{(t)} + n\gamma_{sz}^{(1)}] + \sigma_{nz}\gamma_{nz}^{(0)} \right\}_{(i)} dndsdz \\ U &= \frac{1}{2} \int_0^L \oint_C \left\{ N_{zz}\epsilon_{zz}^{(0)} + L_{zz}\epsilon_{zz}^{(1)} + N_{sz}[\gamma_{sz}^{(0)} + \gamma_{sz}^{(t)}] \right. \\ &\quad \left. + L_{sz}\gamma_{sz}^{(1)} + N_{nz}\gamma_{nz}^{(0)} \right\} dsdz \end{aligned} \quad (2.42)$$

Inserting the strain expressions given by Eqs. 2.15, 2.16 and 2.19 - 2.22 into the energy expression and integrating around the mid-line contour C yields the following strain energy expression

$$\begin{aligned} U &= \frac{1}{2} \int_0^L \left\{ T_z w'_0 + M_z \phi' - B_w \phi'' \right. \\ &\quad + \delta_s [M_x \theta'_x + M_y \theta'_y + Q_x(u'_0 + \theta_y) + Q_y(v'_0 + \theta_x)] \\ &\quad \left. + \delta_{NS} [-M_x v''_p - M_y u''_p] \right\} dz \end{aligned} \quad (2.43)$$

Above energy expression contains tracers δ_S and δ_{NS} which shape the strain energy for two different models, shearable and unshearable, respectively. The detailed information regarding these two models is not included in this section. The details concerning these models is given in the following Free Vibration chapter.

The one dimensional stress resultants and stress couples in the strain expression are given as

$$T_z(z, t) = \oint_C N_{zz} ds \quad (2.44)$$

$$Q_x(z, t) = \delta_S \oint_C \left(\frac{dx}{ds} N_{sz} + \frac{dy}{ds} N_{zn} \right) ds \quad (2.45)$$

$$Q_y(z, t) = \delta_S \oint_C \left(\frac{dy}{ds} N_{sz} - \frac{dx}{ds} N_{zn} \right) ds \quad (2.46)$$

$$M_x(z, t) = \oint_C \left(x N_{zz} + \frac{dy}{ds} L_{zz} \right) ds \quad (2.47)$$

$$M_y(z, t) = \oint_C \left(y N_{zz} - \frac{dx}{ds} L_{zz} \right) ds \quad (2.48)$$

$$M_z(z, t) = \oint_C [\psi(s) N_{zz} + 2\delta_S L_{sz}] ds \quad (2.49)$$

$$B_w(z, t) = \oint_C [F_w(s) N_{zz} - r_t(s) L_{zz}] ds \quad (2.50)$$

$$\begin{aligned} \delta U = & \left[T_z \delta w_0 + (B'_w + M_z) \delta \phi - B_w \delta \phi' \right. \\ & + \delta_S (Q_x \delta u_P + Q_y \delta v_P + M_x \delta \theta_x + M_y \delta \theta_y) \\ & \left. + \delta_{NS} (M'_x \delta v_P + M'_y \delta u_P + M_x \delta v'_P + M_y \delta u'_P) \right]_{z=0}^L \\ & - \int_0^L \left\{ T'_z \delta w_0 + (B''_w + M'_z) \delta \phi + \delta_S [Q'_x \delta u_P + Q'_y \delta v_P \right. \\ & \left. + (M'_x - Q_y) \delta \theta_x + (M'_y - Q_x) \delta \theta_y] + \delta_{NS} [M''_x \delta v_P + M''_y \delta u_P] \right\} dz \end{aligned} \quad (2.51)$$

Here, the expressions represent axial force, shear forces, bending moments, twist moment (Saint-Venant moment) and warping torque (bimoment) respectively. The unit of T_z , Q_x , Q_y is *force*, while M_x , M_y , M_z have the unit of *force.length*. The remaining bimoment B_w has the unit of *force.length²*.

The virtual variation of the displacements in the strain energy δU is taken as Eq. 2.51. Integration by parts is applied to above expression in order to obtain the virtual displacements without any differentiation.

2.1.4.2 Kinetic energy

The kinetic energy expression of the beam is written in terms of density and resultant velocity

$$K = \frac{1}{2} \int_V \rho_{(i)} (\dot{u}^2 + \dot{v}^2 + \dot{w}^2) dV \quad (2.52)$$

Substituting the displacements u , v and w

$$K = \frac{1}{2} \int_V \rho_{(i)} \left\{ [\dot{u}_P - (Y - y_P)\dot{\phi}]^2 + [\dot{v}_P + (X - x_P)\dot{\phi}]^2 + [\dot{w}_0 + X\dot{\theta}_y + Y\dot{\theta}_x - F_w(s)\dot{\phi}' + nr_t(s)\dot{\phi}']^2 \right\} dV \quad (2.53)$$

Also it is known that $X = x + n \frac{dy}{ds}$ and $Y = y - n \frac{dx}{ds}$. Expanding the terms yields a very complex and long expression. Integration through the wall thickness and around mid-line contour requires a lot of formidable calculations. Therefore a parametric programming software, Mathematica is used to handle calculations. As a result, reduced mass terms are introduced and given in Appendix A. Also it has to be mentioned that these mass terms are valid for only symmetrically laminated beams with pole point P at origin.

For symmetrically laminated beams, the mass terms are given as

$$(m_0, m_2) = \sum_{i=1}^N \int_{n_{(i-1)}}^{n_{(i)}} \rho_{(i)} (1, n^2) dn \quad (2.54)$$

The variational kinetic energy is

$$\int_{t_0}^{t_1} \delta \bar{K} dt = - \int_{t_0}^{t_1} \int_V \rho_{(i)} (\ddot{u} \delta u + \ddot{v} \delta v + \ddot{w} \delta w) dV dt \quad (2.55)$$

Arranging the above expression with introducing K_i terms, the variation may be written

$$\begin{aligned} \int_{t_0}^{t_1} \delta \bar{K} dt = & - \int_{t_0}^{t_1} dt \int_0^L \left\{ K_1 \delta u_0 + K_2 \delta v_0 + K_3 \delta w_0 + (K_4 - K_7') \delta \phi \right. \\ & + \delta_{NS} [K_5' \delta u_0 + K_6' \delta v_0] + \delta_S [K_6 \delta \theta_x + K_5 \delta \theta_y] dz \\ & \left. - \int_{t_0}^{t_1} dt \left[K_7 \delta \phi + \delta_{NS} (K_5 \delta u_0 + K_6 \delta v_0) \right] \right\} \Big|_{z=0,L} \end{aligned} \quad (2.56)$$

The K_i terms are given below with corresponding reduced mass terms

$$K_1 = b_1 \ddot{u}_0 - b_2 \ddot{\phi} \quad (2.57)$$

$$K_2 = b_1 \ddot{v}_0 + b_3 \ddot{\phi} \quad (2.58)$$

$$K_3 = b_1 \ddot{w}_0 - b_7 \ddot{\phi}' + \delta_S (b_2 \ddot{\theta}_x + b_3 \ddot{\theta}_y) + \delta_{NS} (-b_2 \ddot{v}_0' - b_3 \ddot{u}_0') \quad (2.59)$$

$$K_4 = b_3 \ddot{v}_0 - b_2 \ddot{u}_0 + (b_4 + b_5 + b_{14} + b_{15}) \ddot{\phi} \quad (2.60)$$

$$\begin{aligned} K_5 = & b_3 \ddot{w}_0 - (b_9 - b_{17}) \ddot{\phi}' + \delta_S [(b_6 - b_{13}) \ddot{\theta}_x + (b_5 + b_{15}) \ddot{\theta}_y] \\ & + \delta_{NS} [-(b_6 - b_{13}) \ddot{v}_0' - (b_5 + b_{15}) \ddot{u}_0'] \end{aligned} \quad (2.61)$$

$$\begin{aligned} K_6 = & b_2 \ddot{w}_0 - (b_8 + b_{16}) \ddot{\phi}' + \delta_S [(b_4 + b_{14}) \ddot{\theta}_x + (b_6 - b_{13}) \ddot{\theta}_y] \\ & + \delta_{NS} [-(b_4 + b_{14}) \ddot{v}_0' - (b_6 - b_{13}) \ddot{u}_0'] \end{aligned} \quad (2.62)$$

$$\begin{aligned} K_7 = & -b_7 \ddot{w}_0 + (b_{10} + b_{18}) \ddot{\phi}' + \delta_S [-(b_8 + b_{16}) \ddot{\theta}_x - (b_9 - b_{17}) \ddot{\theta}_y] \\ & + \delta_{NS} [(b_8 + b_{16}) \ddot{v}_0' + (b_9 - b_{17}) \ddot{u}_0'] \end{aligned} \quad (2.63)$$

$$K_8 = -b_3 \ddot{u}_0 - b_2 \ddot{v}_0 \quad (2.64)$$

Again these K_i functions and the variation of kinetic energy have tracers of δ_{NS} and δ_S . As mentioned before, they classify the system as shearable or unshearable models which detailed explanation of these models is given in the following chapter.

Since this study focuses on the free vibration problem, the work done by external loads such as surface loads, end tractions and body forces are not included in this study.

2.1.5 Equations of Motion

The equations of motion is obtained by Hamilton's principle as well as boundary conditions. The most general equations of motion and boundary conditions for a thin-walled composite beam are given below with tracers of δ_S and δ_{NS} again

$$\delta u_0 : \quad -K_1 + p_x + \delta_S Q'_x + \delta_{NS}(-K'_5 + m'_y + M''_y) = 0 \quad (2.65)$$

$$\delta v_0 : \quad -K_2 + p_y + \delta_S Q'_y + \delta_{NS}(-K'_6 + m'_x + M''_x) = 0 \quad (2.66)$$

$$\delta w_0 : \quad -K_3 + p_z + T'_z = 0 \quad (2.67)$$

$$\delta \phi : \quad -K_4 + K'_7 + b'_w + m_z + B''_w + M'_z = 0 \quad (2.68)$$

$$\delta \theta_x : \quad \delta_S(-K_6 + m_x - Q_y + M'_x) = 0 \quad (2.69)$$

$$\delta \theta_y : \quad \delta_S(-K_5 + m_y - Q_x + M'_y) = 0 \quad (2.70)$$

The boundary conditions at the root and the tip section of the beam are derived through the non-integral terms in the strain energy expression. They are defined at $z = 0$ and $z = L$ as

$$\delta u_0 : u_0 = \bar{u}_0 \quad \text{or} \quad -n_z \tilde{Q}_x - \delta_S Q_x + \delta_{NS}(-K_5 + M'_y) = 0 \quad (2.71)$$

$$\delta_{NS} \delta u'_0 : u'_0 = \bar{u}'_0 \quad \text{or} \quad M_y - n_z \tilde{M}'_y = 0 \quad (2.72)$$

$$\delta v_0 : v_0 = \bar{v}_0 \quad \text{or} \quad -n_z \tilde{Q}_y - \delta_S Q_y + \delta_{NS}(-K_6 + M'_x) = 0 \quad (2.73)$$

$$\delta_{NS} \delta v'_0 : v'_0 = \bar{v}'_0 \quad \text{or} \quad M_x - n_z \tilde{M}'_x = 0 \quad (2.74)$$

$$\delta w_0 : w_0 = \bar{w}_0 \quad \text{or} \quad T_z - n_z \tilde{T}_z = 0 \quad (2.75)$$

$$\delta \phi : \phi = \bar{\phi} \quad \text{or} \quad K_9 - n_z \tilde{M}_z + B'_w + M_z = 0 \quad (2.76)$$

$$\delta\phi' : \phi' = \bar{\phi}' \quad \text{or} \quad -n_z\tilde{B}_w + B_w = 0 \quad (2.77)$$

$$\delta_S\delta\theta_x : \theta_x = \bar{\theta}_x \quad \text{or} \quad M_x - n_z\tilde{M}'_x = 0 \quad (2.78)$$

$$\delta_S\delta\theta_y : \theta_y = \bar{\theta}_y \quad \text{or} \quad M_y - n_z\tilde{M}'_y = 0 \quad (2.79)$$

The equations of motion and boundary conditions will be modified in next chapters due to structural configurations and used shearable model. Also, they will be expressed in terms of a_{ij} stiffness quantities which will be introduced in next chapters.

3. FREE VIBRATION

In order to analyze the dynamic behaviour and vibration characteristics of structures, it is imperative to investigate natural frequencies and mode shapes of the systems. With the knowledge of these, dynamic stabilities like structural resonance and flutter may be prevented from occurrence. This section of thesis focuses on free vibration characteristics of thin walled composite beams.

First, structural composite configurations used in thin walled composite beams are examined. Then governing system of equations are obtained regarding implemented structural composite configuration. Then shearable and unshearable theories are elaborated and solution methodology is profoundly explained. Finally, mass and stiffness matrices are obtained and natural frequencies are calculated.

3.1 Structural Composite Configuration

Two structural composite configurations exist while dealing with thin walled composite beams. These structural configurations produce different structural couplings. These configurations firstly introduced in Ref. [3] and named as *Circumferentially Asymmetric Stiffness Configuration*(CAS) and *Circumferentially Uniform Stiffness Configuration*(CUS). Circumferentially Uniform Configuration states that ply angles act as even function while in Circumferentially Asymmetric Stiffness Configuration ply angles act as odd function.

It is important to examine elastically coupled motion of structures in order not to miss out any critical case resulting from coupling. These cases may emerge unexpectedly in practice unless they are carefully considered in design - analysis phase.

Using Circumferentially Uniform Stiffness Configuration gives an opportunity to investigate two different couplings. These couplings are lateral bending-transverse bending-shear and extension-twist, simulating coupled motion. On the other hand,

using Circumferentially Asymmetric Stiffness Configuration, one can investigate the extension-bending-shear and bending-shear-torsion couplings.

The elaborated derivation for CUS configuration investigated in this thesis and given in the next subsection. Its illustration can be seen in Figure 3.1.

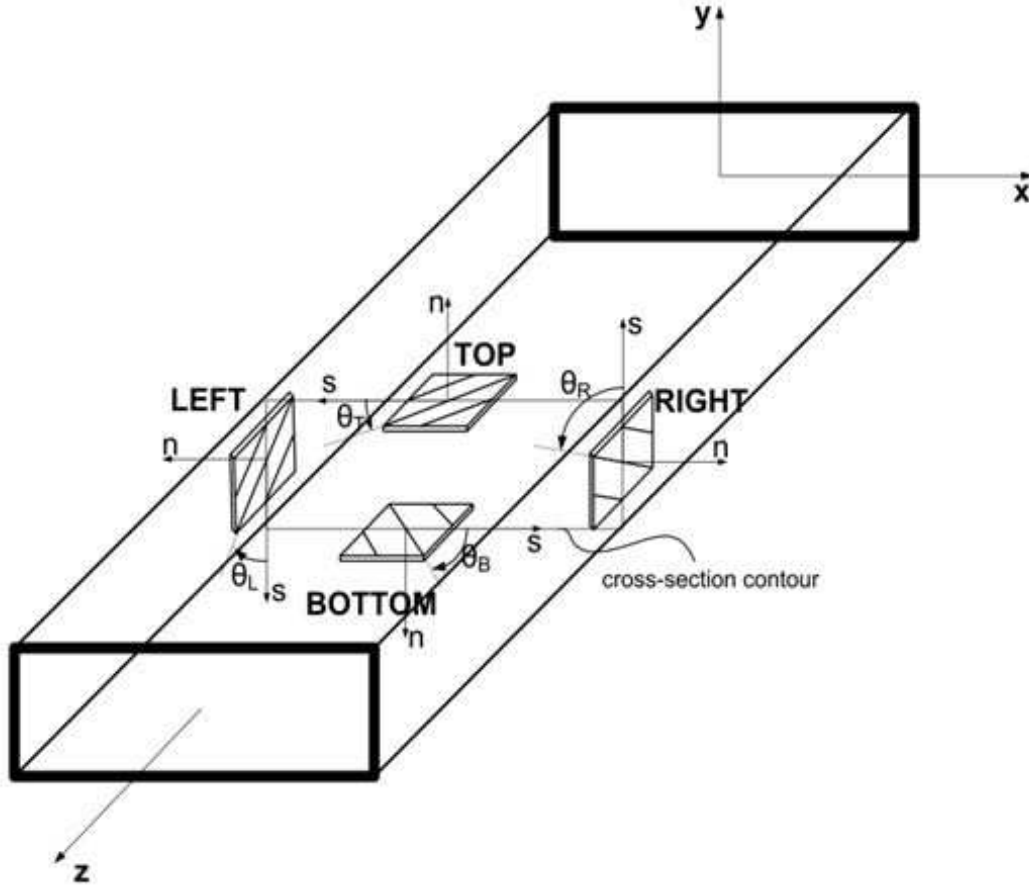


Figure 3.1: CUS configuration

Circumferentially Uniform Stiffness Configuration also referred as antisymmetric configuration exhibits some simplifications in the equations of motion due to its ply angle orientation. These simplifications are simply given below.

The stiffness quantities of \bar{C}_{16} , \bar{C}_{26} , \bar{C}_{36} , \bar{C}_{45} have the same sign with its counterpart in opposite wall. This valid for top-bottom and left-right walls. Simply,

$$\bar{C}_{16}^{(T)} = \bar{C}_{16}^{(B)}; \quad \bar{C}_{26}^{(T)} = \bar{C}_{26}^{(B)}; \quad \bar{C}_{36}^{(T)} = \bar{C}_{36}^{(B)}; \quad \bar{C}_{45}^{(T)} = \bar{C}_{45}^{(B)} \quad (3.1)$$

$$\bar{C}_{16}^{(L)} = \bar{C}_{16}^{(R)}; \quad \bar{C}_{26}^{(L)} = \bar{C}_{26}^{(R)}; \quad \bar{C}_{36}^{(L)} = \bar{C}_{36}^{(R)}; \quad \bar{C}_{45}^{(L)} = \bar{C}_{45}^{(R)} \quad (3.2)$$

This relation also applies to A_{ij} 's, extensional stiffness quantities, and D_{ij} 's, bending stiffness quantities. They are given as

$$\bar{A}_{16}^{(T)} = \bar{A}_{16}^{(B)}; \quad \bar{A}_{26}^{(T)} = \bar{A}_{26}^{(B)}; \quad \bar{A}_{36}^{(T)} = \bar{A}_{36}^{(B)}; \quad \bar{A}_{45}^{(T)} = \bar{A}_{45}^{(B)} \quad (3.3)$$

$$\bar{A}_{16}^{(L)} = \bar{A}_{16}^{(R)}; \quad \bar{A}_{26}^{(L)} = \bar{A}_{26}^{(R)}; \quad \bar{A}_{36}^{(L)} = \bar{A}_{36}^{(R)}; \quad \bar{A}_{45}^{(L)} = \bar{A}_{45}^{(R)} \quad (3.4)$$

$$\bar{D}_{16}^{(T)} = \bar{D}_{16}^{(B)}; \quad \bar{D}_{26}^{(T)} = \bar{D}_{26}^{(B)}; \quad \bar{D}_{36}^{(T)} = \bar{D}_{36}^{(B)}; \quad \bar{D}_{45}^{(T)} = \bar{D}_{45}^{(B)} \quad (3.5)$$

$$\bar{D}_{16}^{(L)} = \bar{D}_{16}^{(R)}; \quad \bar{D}_{26}^{(L)} = \bar{D}_{26}^{(R)}; \quad \bar{D}_{36}^{(L)} = \bar{D}_{36}^{(R)}; \quad \bar{D}_{45}^{(L)} = \bar{D}_{45}^{(R)} \quad (3.6)$$

These ply angle configuration may also be implemented into the open section thin-walled beams. However, this subject is not an interest of this thesis and it is not included.

3.2 Governing Equations of Motion

It is stated that the aircraft wing is modelled as a thin-walled composite beam with Circumferentially Uniform Stiffness structural configuration. The beam is cantilever at the root, $z = 0$, free at the tip, $z = L$. In the subsequent subsections, the equations of motion for a defined beam above can be found investigating two different couplings.

In order to arrange the equations for structural configurations and coupling, new stiffness quantities are resorted. These stiffness quantities are denoted as a_{ij} 's and they are obtained by introducing displacement quantities into the equations of motion. Each of a_{ij} defines a different coupling and their expression are given in Appendix A, specifying which coupling they are involved.

Their calculations are related to some other quantities studied in previous chapters of this thesis. In order to clarify and prevent a confusion about calculations, a chart is provided in Figure 3.2.

3.2.1 Extension-Twist Coupled Motion

The equations of motion for extension-twist coupling is given in here. The solution to these equation is not included in the thesis. The equations are introduced only to give an idea about the motion of the beam for this coupling.

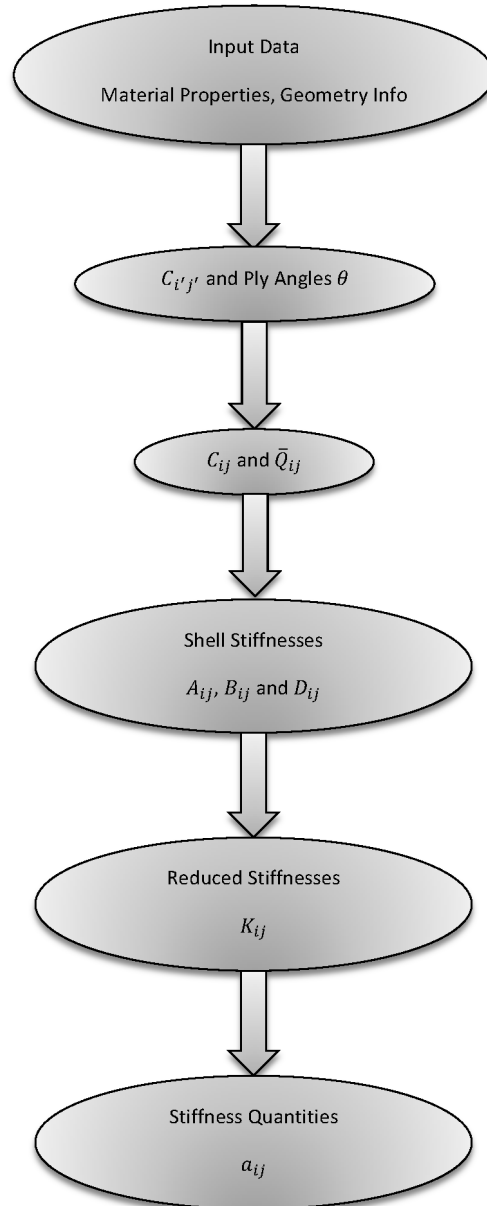


Figure 3.2: Evaluation of the stiffness quantities, a_{ij}

The governing equations of motion for extension-twist are

$$\delta w_0 : \quad a_{11}w_0'' + a_{17}\phi'' = b_1\ddot{w}_0 \quad (3.7)$$

$$\delta \phi : \quad -a_{66}\phi'''' + a_{77}\phi'' + a_{17}w_0'' = [(b_4 + b_5) + \delta_n(b_{14} + b_{15})]\ddot{\phi} - (b_{10} + \delta_nb_{18})\ddot{\phi}'' \quad (3.8)$$

The boundary conditions at root, $z = 0$

$$w_0 = 0; \quad \phi = 0; \quad \phi' = 0 \quad (3.9)$$

The boundary conditions at tip, $z = L$

$$\delta w_0 : \quad a_{11}w_0' + a_{17}\phi' = 0 \quad (3.10)$$

$$\delta \phi : \quad -a_{66}\phi''' + a_{77}\phi' + a_{17}w_0' = -(b_{10} + \delta_nb_{18})\phi' \quad (3.11)$$

$$\delta \phi' : \quad a_{66}\phi'' = 0 \quad (3.12)$$

Here, tracer δ_n denotes secondary warping effects and in this study those effects are taken into account. Therefore tracer δ_n takes value of 1.

3.2.2 Lateral Bending-Transverse Bending-Shear Coupled Motion

In this section, the equations of motion of a thin-walled composite beam is given for lateral bending-transverse bending-shear coupling. The equations are treated with two models, shearable and unshearable models, respectively.

The tracer of δ_n is mentioned in previous chapter. Its function is the same and takes value of 1.

3.2.2.1 Shearable model

This model includes shear effects and consists of 49 stiffness quantities, 28 independent and 21 off-diagonal (coupling). As it can be interpreted from the numbers, this model relatively difficult due to inclusion of shear effects.

The equations of motion for shearable model

$$\delta u_0 : \quad a_{34}\theta_x'' + a_{44}(u_0'' + \theta_y') = b_1\ddot{u}_0 \quad (3.13)$$

$$\delta v_0 : \quad a_{25}\theta_y'' + a_{55}(v_0'' + \theta_x') = b_1\ddot{v}_0 \quad (3.14)$$

$$\delta \theta_x : \quad a_{33}\theta_x'' + a_{34}(u_0'' + \theta_y') - a_{55}(v_0' + \theta_x) - a_{25}\theta_y' = (b_4 + \delta_n b_{14})\ddot{\theta}_x \quad (3.15)$$

$$\delta \theta_y : \quad a_{22}\theta_y'' + a_{25}(v_0'' + \theta_x') - a_{44}(u_0' + \theta_y) - a_{34}\theta_x' = (b_5 + \delta_n b_{15})\ddot{\theta}_y \quad (3.16)$$

The boundary conditions at root, $z = 0$

$$u_0 = 0; \quad v_0 = 0; \quad \theta_x = 0; \quad \theta_y = 0 \quad (3.17)$$

The boundary conditions at tip, $z = L$

$$\delta u_0 : \quad a_{34}\theta_x' + a_{44}(u_0' + \theta_y) = 0 \quad (3.18)$$

$$\delta v_0 : \quad a_{25}\theta_y' + a_{55}(v_0' + \theta_x) = 0 \quad (3.19)$$

$$\delta \theta_x : \quad a_{33}\theta_x' + a_{34}(u_0' + \theta_y) = 0 \quad (3.20)$$

$$\delta \theta_y : \quad a_{22}\theta_y' + a_{25}(v_0' + \theta_x) = 0 \quad (3.21)$$

3.2.2.2 Unshearable model

In this model, transverse and lateral shear effects are discarded which makes the model relatively simple. The fundamental difference results from letting $\theta_y \rightarrow -u_p'$ and $\theta_x \rightarrow -v_p'$ and some arrangements. This model consists of 15 independent and 10 off-diagonal (coupling) stiffness quantities, a total number of 25.

The equations of motion for unshearable model

$$\delta u_P : \quad a_{22}u_P'''' = [(b_5 + \delta_n b_{15})\ddot{u}_P]' - b_1\ddot{u}_P \quad (3.22)$$

$$\delta v_P : \quad a_{33}v_P'''' = [(b_4 + \delta_n b_{14})\ddot{v}_P]' - b_1\ddot{v}_P \quad (3.23)$$

The boundary conditions at root, $z = 0$

$$u_P = 0; \quad u_P' = 0; \quad v_P = 0; \quad v_P' = 0 \quad (3.24)$$

The boundary conditions at tip, $z = L$

$$\delta u_P : (a_{22}u_P'')' - (b_5 + \delta_n b_{15})\ddot{u}_P' = 0 \quad (3.25)$$

$$\delta u_P' : a_{22}u_P'' = 0 \quad (3.26)$$

$$\delta v_P : (a_{33}v_P'')' - (b_4 + \delta_n b_{14})\ddot{v}_P' = 0 \quad (3.27)$$

$$\delta v_P' : a_{33}v_P'' = 0 \quad (3.28)$$

3.3 Solution Methodology

In this section solution methodology is explained in a detailed way and the shearable equations of motion for lateral bending-transverse bending-shear coupling are solved. The governing equations of motion for thin-walled composite beams obtained in previous section is considerably complex and can not be solved analytically. Therefore, a numerical method, Extended Galerkin Method, is employed here to obtain a solution for the equations of motion. In this method, the trial functions are selected only to satisfy the geometric boundary conditions [17]. They are also called admissible functions and are chosen as polynomials orders of approximately 7-9. Extended Galerkin Method applies a discretization to displacements as below

$$u_0(z, t) = N_u^T(z)q_u(t) \quad (3.29)$$

$$v_0(z, t) = N_v^T(z)q_v(t) \quad (3.30)$$

$$\theta_x(z, t) = N_x^T(z)q_x(t) \quad (3.31)$$

$$\theta_y(z, t) = N_y^T(z)q_y(t) \quad (3.32)$$

Here, N 's are shape functions and have dimension of $N \times 1$ while q 's are generalized coordinates with dimension of $1 \times N$. Then the discretized equations of motion can be rearranged as

$$\mathbf{M}\ddot{\mathbf{q}}(t) + \mathbf{K}\mathbf{q}(t) = \mathbf{Q}(t) \quad (3.33)$$

To perform free vibration analysis, it is assumed that beam has simple harmonic motion, $q = X e^{i\omega t}$, and external loads are eliminated, $\mathbf{Q}(t) = 0$, which yields eigenvalue problems

$$\mathbf{M}\ddot{\mathbf{q}}(t) + \mathbf{K}\mathbf{q}(t) = 0 \quad (3.34)$$

$$(\lambda \mathbf{I} - \mathbf{M}^{-1}\mathbf{K})\mathbf{X} = 0 \quad (3.35)$$

Here λ and \mathbf{X} represents eigenvalues and eigenvectors, respectively. The natural frequencies can be computed by the relation of $\lambda = \omega^2$ while eigenvectors are indicating mode shapes.

Mass and stiffness matrices are also calculated with the help of Extended Galerkin Method as only functions of spanwise coordinate, z . The matrices are given as

$$\mathbf{M} = \int_0^L \begin{bmatrix} b_1 N_u N_u^T & 0 & 0 & 0 \\ 0 & b_1 N_v N_v^T & 0 & 0 \\ 0 & 0 & (b_4 + b_{14}) N_x N_x^T & 0 \\ 0 & 0 & 0 & (b_5 + b_{15}) N_y N_y^T \end{bmatrix} dz \quad (3.36)$$

$$\mathbf{K} = \int_0^L \begin{bmatrix} a_{44} N'_u N'^T_u & 0 & a_{34} N'_u N'^T_x & a_{44} N'_u N'^T_y \\ 0 & a_{55} N'_v N'^T_v & a_{55} N'_v N'^T_x & a_{25} N'_v N'^T_y \\ a_{34} N'_x N'^T_u & a_{55} N'_x N'^T_v & a_{33} N'_x N'^T_x + a_{55} N_x N_x^T & a_{34} N'_x N'^T_y + a_{52} N_x N_y^T \\ a_{44} N'_y N'^T_u & a_{25} N'_y N'^T_v & a_{25} N'_y N'^T_x + a_{34} N_y N_x^T & a_{22} N'_y N'^T_y + a_{44} N_y N_y^T \end{bmatrix} dz \quad (3.37)$$

Besides, the generalized coordinates are given as

$$\mathbf{q} = \{q_u \ q_v \ q_x \ q_y\}^T \quad (3.38)$$

3.4 Results and Discussion

The preliminary results are presented for the dynamic analysis of the thin-walled composite beams. Firstly, the validation of the mathematical model is performed. For this purpose, natural frequencies are obtained for a thin-walled box beam whose properties are given in the Table 3.1 and the results are tabulated for selected ply angles in Table 3.2

Table 3.2 shows the results for the first four natural frequencies which corresponds to vertical and lateral bending modes of the box beam. As seen, an excellent agreement between the presented results and the ones provided by Ref. [1] is obtained, providing validation of generated mathematical model.

Also in Figure 3.3, the stiffness quantities, a_{ij} 's, of thin-walled composite box beam are plotted for selected ply angles. Moreover, Figure 3.4 and Figure 3.5 show the variation of first two transverse and lateral natural frequencies versus ply angle, respectively.

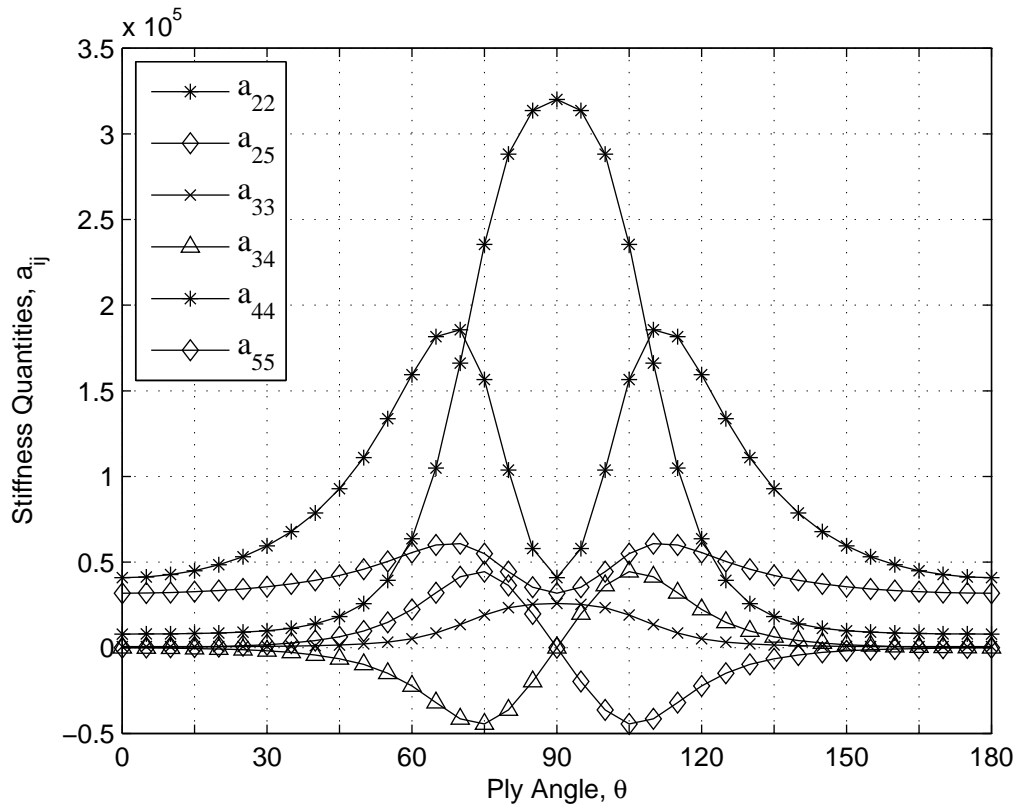


Figure 3.3: Variation of stiffness quantities versus ply angles

Table 3.1: Material Properties and Geometric Dimensions of The Box Beam

Graphite-Epoxy	
E_{11}	206.75 GPa
$E_{22} = E_{33}$	5.17 GPa
G_{12}	3.10 GPa
$G_{13} = G_{23}$	2.55 GPa
$\nu_{21} = \nu_{31}$	0.00625
ν_{32}	0.25
Density, ρ	1528.15 kg/m ³
Geometry	
Width, $2b$	0.0254 m
Depth, $2d$	0.00508 m
Thickness, h	0.001016 m
Length, L	0.254 m
Number of Layers	6

Table 3.2: Comparison of First Natural Frequencies for Box Beam

Ply Angle θ (Degree)	$\omega_{horizontal}$ (rad/s)	$\omega_{horizontal}$ (rad/s) Ref. [1]	$\omega_{vertical}$ (rad/s)	$\omega_{vertical}$ (rad/s) Ref. [1]
0	842.89	843	241.4	241
	4193.02	4193	1506.75	1507
15	857.36	857	245.06	245
	4255.90	4256	1529.57	1530
30	935.46	935	263.08	263
	4562.69	4563	1641.94	1642
45	1234.83	1235	314.33	314
	5424.28	5424	1962.15	1962
60	2174.23	2174	439.75	440
	7491.19	7491	2763.99	764
75	3907.77	3908	761.00	761
	12272.81	12273	4912.88	4913
90	4579.59	4580	1499.36	1499
	18056.78	18057	8503.90	8503

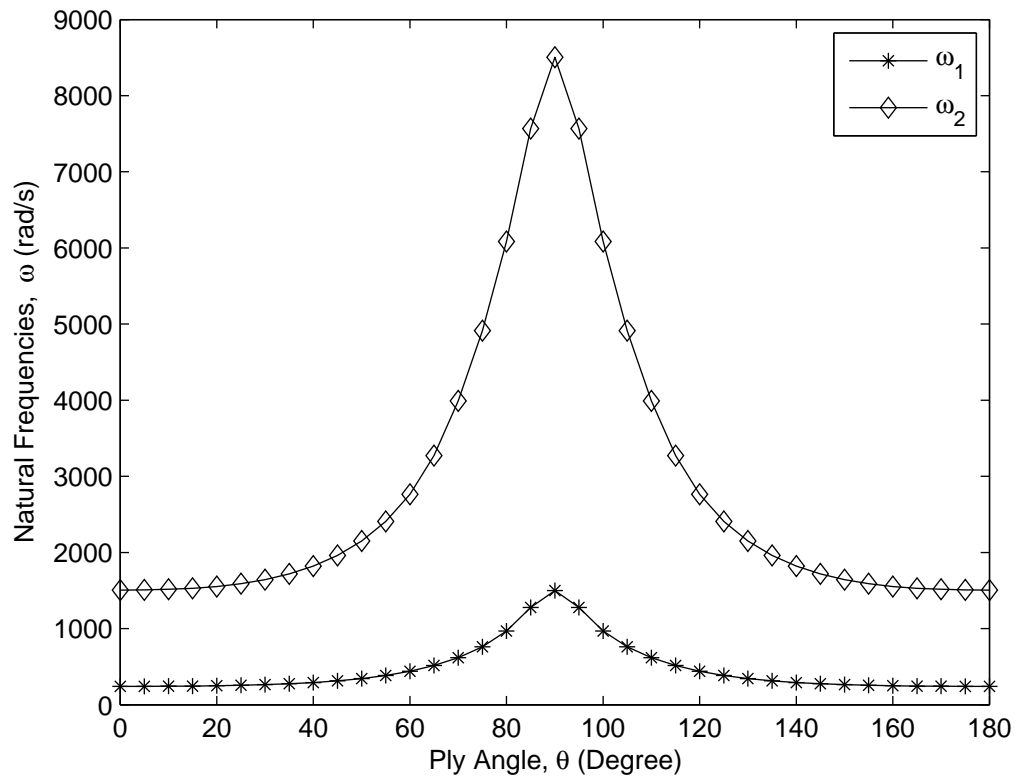


Figure 3.4: First two natural frequencies of vertical bending mode of the box beam

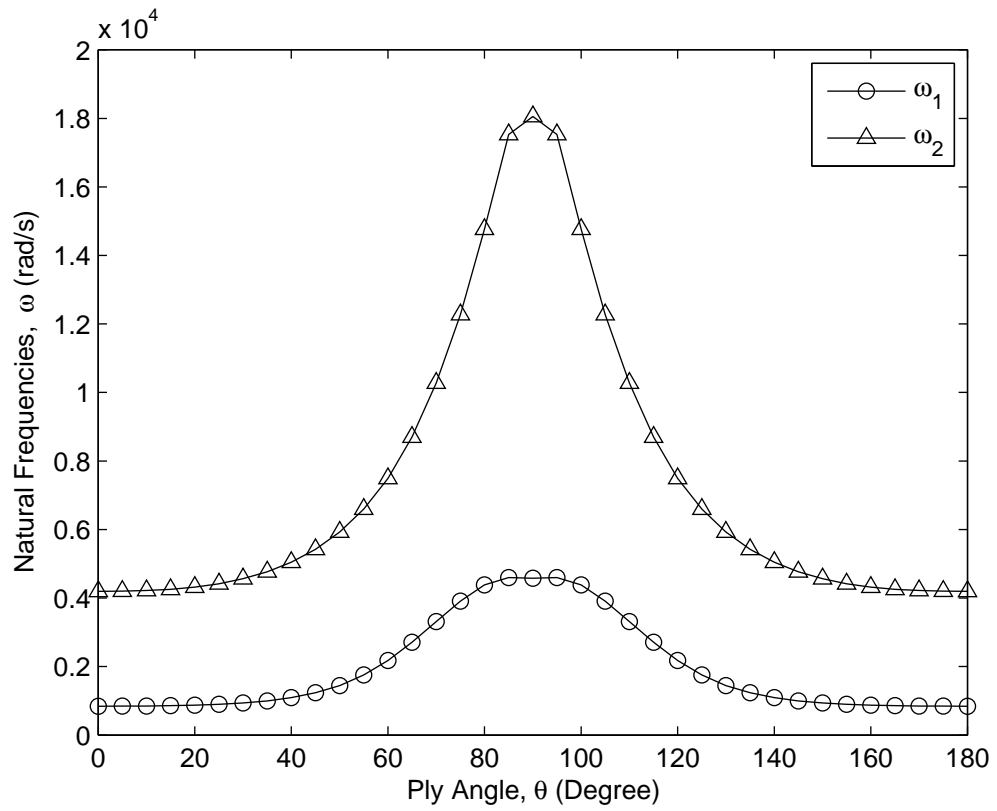


Figure 3.5: First two natural frequencies of lateral bending mode of the box beam

The next analyses are conducted for the thin-walled composite beam with a diamond shaped cross section. Keeping the material properties same, the width and depth of the beam are taken as 0.254m, the thickness of the beam and length are chosen as 0.01m and 2.032m, respectively. The geometry of the diamond shaped wing can be seen in Fig 3.6. Material properties are kept as the same. The results are given in the following figures.

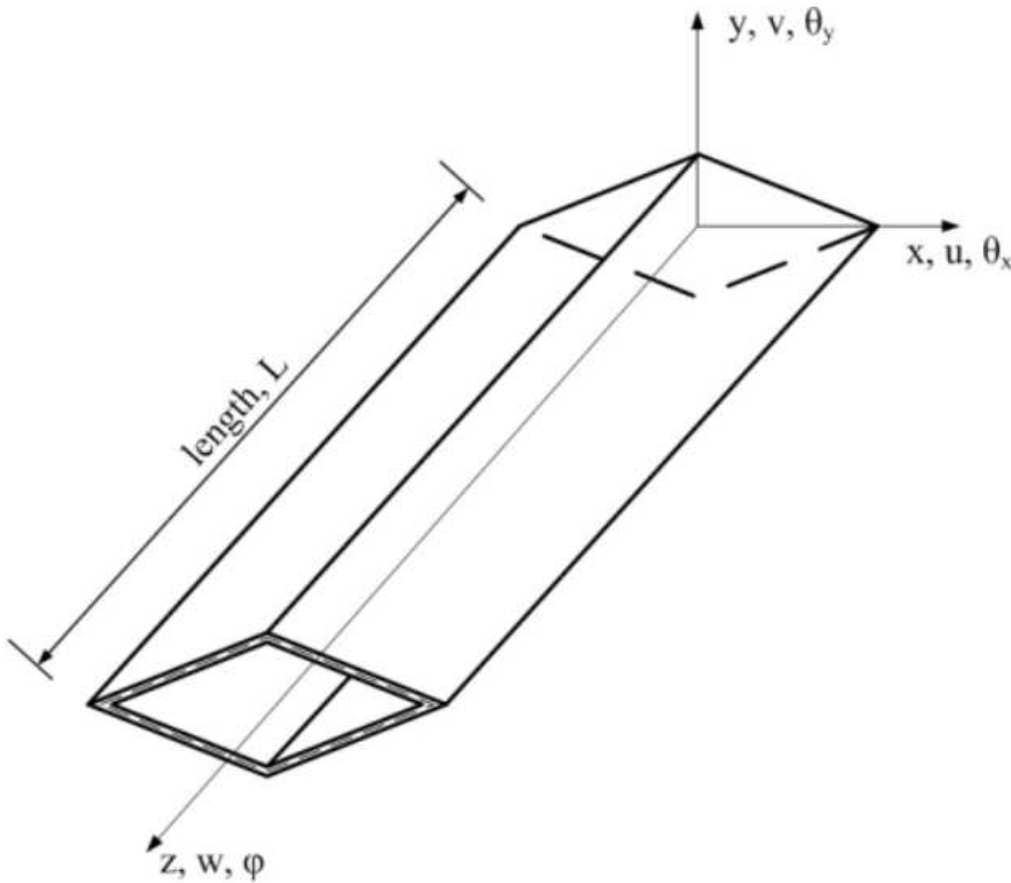


Figure 3.6: The geometry of the diamond shaped thin walled beam

Figure 3.7 depicts the stiffness quantities, a_{ij} of diamond shaped thin-walled composite beam. It is seen from the Figure, bending stiffness quantities are dominant compared to others.

Figure 3.8 shows the variation of first two natural frequencies of the diamond shaped beam. Due to equal depth and width of the cross-section, the natural frequency results of the lateral and transverse bending modes overlap with each other.

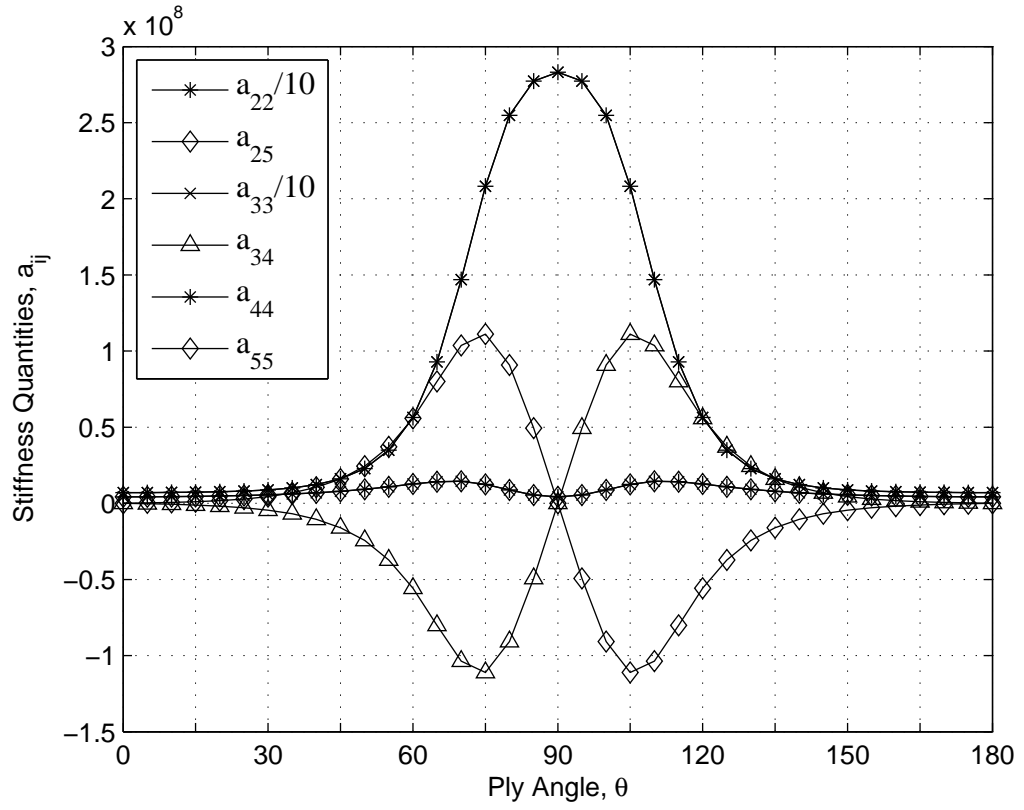


Figure 3.7: Stiffness quantities for diamond shaped thin-walled beam

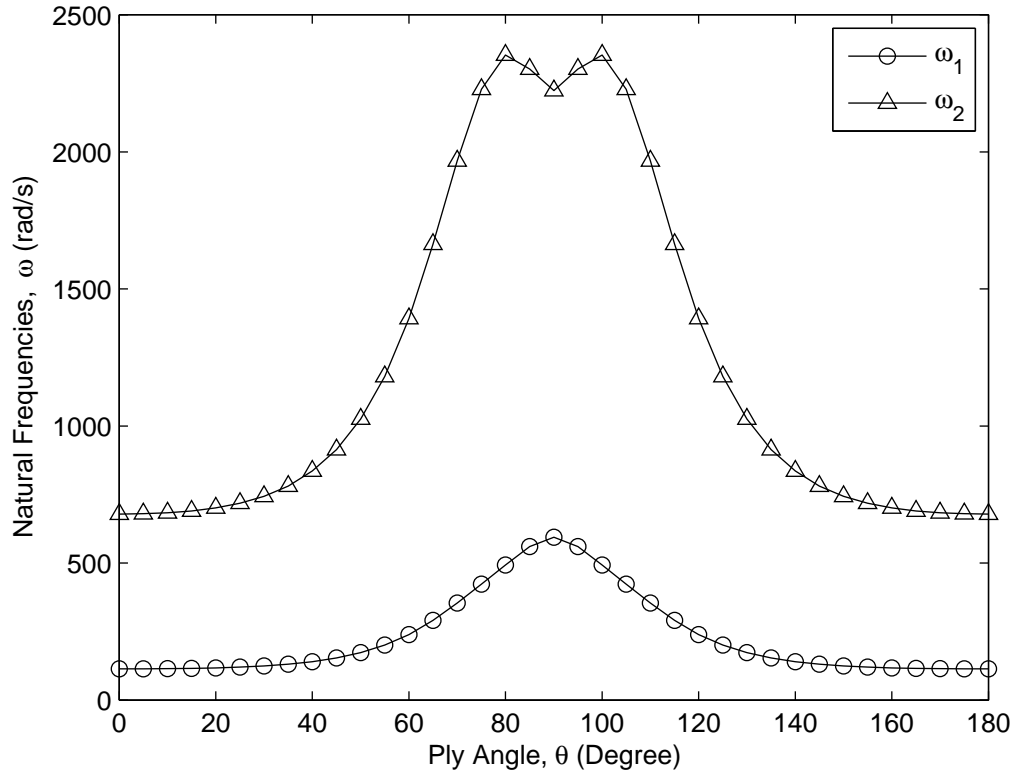


Figure 3.8: First two natural frequencies of the diamond shaped thin-walled beam

4. ACTIVE VIBRATION CONTROL

Active vibration control is an active application, using some control gain, that reacts to ongoing vibrations by applying excitation on the opposite way of the forces caused by vibration. Using this application, it is possible to enhance damping characteristics and prevent structural instabilities such as structural resonance. Moreover, undesired noise can also be avoided. One way to achieve vibration control appears from use of adaptive materials. Adaptive or smart materials such as piezoelectric materials has a wide range of use recently. They are likely to have a great importance in the design process of aerospace structural systems, robot manipulators and helicopter rotor blades. Using these latest concept, new generation of structural systems can be designed to operate safely in fierce environments.

Piezoelectric materials are recently introduced materials into the structures, capable of generating mechanical strain under applied voltage. They are found in nature as polymers or composite ceramics and they can be implemented into structures as sensors and actuators, in order to control the structure in a predictable manner. There are two different piezoelectric effects, namely direct and converse. The first one refers to electrical charge generation as a result of applied mechanical force while the latter one referring to generation of mechanical strain/moment due to applied electrical field or voltage. In this study, converse piezoelectric effect is used and bending moments are induced as a result of applied voltage. Also, piezoelectric materials are used as both sensors and actuators in order to achieve closed-loop feedback control law.

The piezoelectrically induced bending moments can occur in both directions and they are represented with \tilde{M}_x and \tilde{M}_y . Their expressions are given as [8]

$$\begin{aligned} \tilde{M}_x = & \int \xi_3(n_+ - n_-)\bar{e}_{31}R(s,z) \left[y(1 - \frac{A_{12}^*}{A_{11}^*}) + \frac{dx}{ds} \frac{B_{12}^*}{A_{11}^*} \right] ds \\ & - \frac{1}{2} \int \left[\frac{dx}{ds} \xi_3(n_+^2 - n_-^2)\bar{e}_{31}R(s,z) \right] ds \end{aligned} \quad (4.1)$$

$$\begin{aligned}\tilde{M}_y = & \int \xi_3(n_+ - n_-)\bar{e}_{31}R(s,z) \left[x\left(1 - \frac{A_{12}^*}{A_{11}^*}\right) + \frac{dy}{ds} \frac{B_{12}^*}{A_{11}^*} \right] ds \\ & - \frac{1}{2} \int \left[\frac{dy}{ds} \xi_3(n_+^2 - n_-^2)\bar{e}_{31}R(s,z) \right] ds\end{aligned}\quad (4.2)$$

Here n_+ and n_- represents the upper and lower faces of the piezoelectric layer, respectively. Besides, A_{ij}^* and B_{ij}^* denote the local stiffness quantities related to piezoactuators.

From Equation 4.1 and 4.2, it is seen that induced moments are proportional to applied electrical field. Therefore, the moment expressions can be rewritten simply,

$$\tilde{M}_x = \xi_3 C_{M_x}; \quad \tilde{M}_y = \xi_3 C_{M_y} \quad (4.3)$$

where expressions of C_{M_x} and C_{M_y} are obvious from previous equations. Then global moment expressions can be arranged as

$$M_x = M'_x - \tilde{M}_x; \quad M_y = M'_y - \tilde{M}_y \quad (4.4)$$

where $'$ denotes mechanical moments. Therefore, equations of motion with influence of piezoelectrically induced moments are given as below in most general case

$$\delta u_0 : \quad a_{34}\theta_x'' + a_{44}(u_0'' + \theta_y') - b_1\ddot{u}_0 + p_x(x,t) = 0 \quad (4.5)$$

$$\delta v_0 : \quad a_{25}\theta_y'' + a_{55}(v_0'' + \theta_x') - b_1\ddot{v}_0 + p_y(z,t) = 0 \quad (4.6)$$

$$\begin{aligned}\delta \theta_x : \quad & a_{33}\theta_x'' + a_{34}(u_0'' + \theta_y') - a_{55}(v_0' + \theta_x) - a_{25}\theta_y' \\ & - (b_4 + \delta_n b_{14})\ddot{\theta}_x - \delta_P \tilde{M}'_x + m_x(z,t) = 0\end{aligned} \quad (4.7)$$

$$\begin{aligned}\delta \theta_y : \quad & a_{22}\theta_y'' + a_{25}(v_0'' + \theta_x') - a_{44}(u_0' + \theta_y) - a_{34}\theta_x' \\ & - (b_5 + \delta_n b_{15})\ddot{\theta}_y - \delta_P \tilde{M}'_y + m_y(z,t) = 0\end{aligned} \quad (4.8)$$

The boundary conditions at root, $z = 0$,

$$u_0 = 0; \quad v_0 = 0; \quad \theta_x = 0; \quad \theta_y = 0 \quad (4.9)$$

The boundary conditions at tip, $z = L$,

$$\delta u_0 : \quad a_{34}\theta'_x + a_{44}(u'_0 + \theta_y) = 0 \quad (4.10)$$

$$\delta v_0 : \quad a_{25}\theta'_y + a_{55}(v'_0 + \theta_x) = 0 \quad (4.11)$$

$$\delta \theta_x : \quad a_{33}\theta'_x + a_{34}(u'_0 + \theta_y) - \delta_S \tilde{M}_x = 0 \quad (4.12)$$

$$\delta \theta_y : \quad a_{22}\theta'_y + a_{25}(v'_0 + \theta_x) - \delta_S \tilde{M}_y = 0 \quad (4.13)$$

4.1 Boundary Moment Control Law

The location of piezoelectric actuators plays a major role in the design process. The bending moments can be induced by either piezoelectric patches or piezoelectric layers spread all over entire span. As a result of these two different mechanisms, the influence of piezoelectrically induced moments on the equations of motion varies. The tracers in the equations of motion given in previous section are used to model this difference.

The use of piezopatches involves with derivatives of moments and they affect the equations of motion directly. In order to model this concept, tracer δ_N is inserted to equations. For piezopatches the tracer δ_N takes value of 1 while δ_S becomes zero.

The other method is spreading piezoactuators embedded all along the entire beam span. As a result of that, the total induced moment can be obtained after an integration. The total moment acts as a bending moment at the beam tip [1,6,18]. Therefore it does not involve with the equations of motion but boundary conditions at the tip [19]. This is called boundary moment control law. In this concept, tracer δ_S takes value of 1 while δ_N becomes zero.

In this study, boundary moment control law is applied to the system. Therefore, the equations of motion and the boundary conditions can be rearranged with proper values of tracers. In addition, since this study is interested in determination of natural frequencies and their predictable control, external force terms are also cancelled to perform free vibration analyses. Eventually, the equations of motion and the boundary conditions become

$$\delta u_0 : \quad a_{34}\theta_x'' + a_{44}(u_0'' + \theta_y') - b_1\ddot{u}_0 = 0 \quad (4.14)$$

$$\delta v_0 : \quad a_{25}\theta_y'' + a_{55}(v_0'' + \theta_x') - b_1\ddot{v}_0 = 0 \quad (4.15)$$

$$\delta \theta_x : \quad a_{33}\theta_x'' + a_{34}(u_0'' + \theta_y') - a_{55}(v_0' + \theta_x) - a_{25}\theta_y' - (b_4 + \delta_n b_{14})\ddot{\theta}_x = 0 \quad (4.16)$$

$$\delta \theta_y : \quad a_{22}\theta_y'' + a_{25}(v_0'' + \theta_x') - a_{44}(u_0' + \theta_y) - a_{34}\theta_x' - (b_5 + \delta_n b_{15})\ddot{\theta}_y = 0 \quad (4.17)$$

The boundary conditions at root, $z = 0$,

$$u_0 = 0; \quad v_0 = 0; \quad \theta_x = 0; \quad \theta_y = 0 \quad (4.18)$$

The boundary conditions at tip, $z = L$,

$$\delta u_0 : \quad a_{34}\theta_x' + a_{44}(u_0' + \theta_y) = 0 \quad (4.19)$$

$$\delta v_0 : \quad a_{25}\theta_y' + a_{55}(v_0' + \theta_x) = 0 \quad (4.20)$$

$$\delta \theta_x : \quad a_{33}\theta_x' + a_{34}(u_0' + \theta_y) = \tilde{M}_x \quad (4.21)$$

$$\delta \theta_y : \quad a_{22}\theta_y' + a_{25}(v_0' + \theta_x) = \tilde{M}_y \quad (4.22)$$

4.2 Closed Loop Feedback Control Laws

It is mentioned before that piezoelectric materials can be used as sensors, actuators or as both in a system. When they are inserted to a system as both, it is possible to form a closed loop feedback control [7, 8]. Using closed loop feedback control law, with proper value of control gain it is likely to obtain a way better control behaviour, advantageous to open loop control law. The induced bending moments can be regulated to be proportional to the position, the velocity or even the acceleration of the beam tip.

In closed loop controls, the voltage output from the sensors is amplified with the proper gain and fed back to actuators. The electrical charge from sensors is collected from sensors and then redistributed to the actuators again. Thus, this section explains how closed loop control law work.

The electric displacement expression is

$$D_3 = \bar{e}_{31} \epsilon_{zz} \quad (4.23)$$

The electric charge due to displacement

$$q_s(t) = \int_{A_s} D_3 dA_s = \int_{A_s} \bar{e}_{31} \epsilon_{zz} dA_s \quad (4.24)$$

As a result, the sensor output voltage

$$V_s(t) = \frac{q_s(t)}{C_p} \quad (4.25)$$

In above equations, C_p and A_s represent the sensor's capacitance and area, respectively.

It is assumed that sensors are located symmetrically on opposite walls, then Equation 4.23 can be rewritten

$$V_S^x(t) = C_x^S \theta_x(L, t); \quad V_S^y(t) = C_y^S \theta_y(L, t) \quad (4.26)$$

The expression of C^S es is not given here but can be easily obtained from Equations 4.22, 4.23 and 2.14

Two different feedback control laws are applied, namely, proportional and velocity feedback law. They are summarized in next subsections and their related equations are given.

4.2.1 Proportional Feedback Control Law

In proportional feedback control law, the piezoelectrically induced bending moments are proportional to the position of the beam tip node. The information of the position is sensed and transferred to actuator after multiplication with the control gain. Therefore, the induced moment becomes related to position of the beam tip.

Actuating voltage, proportional to the voltage output of sensor

$$\xi_3^x(t) = \frac{k_p V_S^x(t)}{h_a}; \quad \xi_3^y(t) = \frac{k_p V_S^y(t)}{h_a} \quad (4.27)$$

where h_a is the thickness of the piezoelectric layer and k_p is the proportional feedback gain. Then, moment expressions become

$$\tilde{M}_x = -\frac{k_p C_{M_x^a}}{h_a} [C_x^S \theta_x(L, t)] = -k_p C_{11} \theta_x(L, t) \quad (4.28)$$

$$\tilde{M}_y = -\frac{k_p C_{M_y^a}}{h_a} [C_y^S \theta_y(L, t)] = -k_p C_{22} \theta_y(L, t) \quad (4.29)$$

4.2.2 Velocity Feedback Control Law

In velocity feedback control law, the piezoelectrically induced bending moments are proportional to the velocity of the beam tip node. The information of the velocity is sensed and transferred to actuator after multiplication with the control gain. Therefore, the induced moment becomes related to velocity, the time derivative of position, of the beam tip.

Actuating voltage, proportional to the voltage output of sensor

$$\xi_3^x(t) = \frac{k_v dV_S^x(t)/dt}{h_a}; \quad \xi_3^y(t) = \frac{k_v dV_S^y(t)/dt}{h_a} \quad (4.30)$$

where h_a is the thickness of the piezoelectric layer and k_v is the velocity feedback gain. Then, moment expressions become

$$\tilde{M}_x = -\frac{k_v C_{M_x^a}}{h_a} [C_x^S \dot{\theta}_x(L, t)] = -k_v C_{11} \dot{\theta}_x(L, t) \quad (4.31)$$

$$\tilde{M}_y = -\frac{k_v C_{M_y^a}}{h_a} [C_y^S \dot{\theta}_y(L, t)] = -k_v C_{22} \dot{\theta}_y(L, t) \quad (4.32)$$

4.3 Solution Methodology

Solution methodology was explained in the previous chapter. Applying same method, mass and stiffness matrices remain the same while the effects of induced moments are taken into account here. The most general case of virtual work including piezoelectrically induced bending moments

$$\begin{aligned}
\delta J = & \tilde{M}_x(L,t)\delta\theta_x(L,t) + \tilde{M}_y(L,t)\delta\theta_y(L,t) + \int_0^L [p_x^d(z,t)\delta u_0(z,t) \\
& + p_y^d(z,t)\delta v_0(z,t) + m_x^d(z,t)\delta\theta_x(z,t) + p_y^d(z,t)\theta_y(z,t)]dz \\
& + \sum_i [p_x^c(z_i,t)\delta u_0(z_i,t) + p_y^c(z_i,t)\delta v_0(z_i,t) \\
& + m_x^c(z_i,t)\delta\theta_x(z_i,t) + m_y^c(z_i,t)\delta\theta_y(z_i,t)]
\end{aligned} \tag{4.33}$$

The superscripts d and c stand for distributed and concentrated loads, respectively. Depending on the which control law is used, the discretized virtual work for the adaptive beam is

$$\delta J = \mathbf{Q}^T \delta q - \delta_p q^T K_p \mathbf{K}_C \delta q - \delta_v \dot{q}^T K_v \mathbf{K}_C \delta q \tag{4.34}$$

Here, \mathbf{K}_C is the newly introduced control matrix. Also two new tracers, δ_p and δ_v , identify which control law is used. δ_p denotes proportional feedback control law, δ_v stands for velocity feedback law. They take value of 0 or 1 depending on control law.

Therefore, discretized system for closed loop control

$$\mathbf{M}\ddot{q}(t) + \delta_v K_v \mathbf{K}_C \dot{q}(t) + \mathbf{K}q(t) + \delta_p K_p \mathbf{K}_C q(t) = \mathbf{Q}(t) \tag{4.35}$$

This expression is also similar to the one presented by Ref. [20]. Here \mathbf{M} and \mathbf{K} must be taken into consideration for both the host and the piezoactuators as a whole. Stiffness quantities of piezoactuators must be determined and inserted to matrices. Also \mathbf{K}_C matrix is given as

$$\mathbf{K}_C = \begin{bmatrix} 0 & 0 & 0 & 0 \\ 0 & 0 & 0 & 0 \\ 0 & 0 & C_{11}N_x(L)N_x^T(L) & 0 \\ 0 & 0 & 0 & C_{22}N_y(L)N_y^T(L) \end{bmatrix} \tag{4.36}$$

where C_{11} and C_{22} are elastic coefficients of piezoelectric material.

Afterwards, solution is obtained by casting the discretized equation into state-space form as $\mathbf{q}_1 = \dot{\mathbf{q}}$ and $\mathbf{q}_2 = \dot{\mathbf{q}}_1 = \ddot{\mathbf{q}}$. The state space representation can be expressed as

$$\dot{\mathbf{x}}(t) = \mathbf{A}\mathbf{x}(t) + \mathbf{W}_F(t) \quad (4.37)$$

The \mathbf{A} and \mathbf{W}_F matrices are

$$\mathbf{A} = \begin{bmatrix} \mathbf{0} & \mathbf{I} \\ -\mathbf{M}^{-1}\hat{\mathbf{K}} - \delta_v\mathbf{M}^{-1}K_v\mathbf{K}_C \end{bmatrix} \quad (4.38)$$

$$\mathbf{W}_F = \begin{bmatrix} \mathbf{0} \\ -\mathbf{M}^{-1}\mathbf{Q}(t) \end{bmatrix} \quad (4.39)$$

where $\mathbf{0}$ and \mathbf{I} are zero and identity matrices.

$$\hat{\mathbf{K}} = \mathbf{K} + \delta_p K_p \mathbf{K}_C \quad (4.40)$$

To perform free vibration analyses, external forces are assumed to be zero, $\mathbf{Q}(t) = 0$. Then, Equation 4.35 reduces to

$$\dot{\mathbf{x}}(t) = \mathbf{A}\mathbf{x}(t) \quad (4.41)$$

which has a solution in the form of

$$\mathbf{x}(t) = \mathbf{X}e^{\lambda t} \quad (4.42)$$

and yields to an eigenvalue problem

$$\mathbf{A}\mathbf{X} = \lambda \mathbf{X} \quad (4.43)$$

In the absence of velocity feedback gain, $K_v = 0$, the eigenvalues are complex quantities. It is also obvious that one cannot observe structural damping without velocity feedback gain. The eigenvalues and structural damping factor expressions are given as

$$\lambda_r = \eta_r \pm i\omega_d r \quad (4.44)$$

$$\xi_r = \frac{-\eta_r}{\sqrt{\eta_r^2 + \omega_d^2 r}} \quad (4.45)$$

4.4 Results and Discussion

Application of closed loop control laws was discussed in the previous section. This section represents the dynamic results for the thin walled diamond shaped wing. However, prior to these results, a case study has been performed and closed loop control has been implemented on a Timoshenko beam. Results are given and compared to the ones provided by the Ref [21].

4.4.1 Case Study-Timoshenko Beam

In this case study influence of the piezoelectric effects on the natural frequencies of a Timoshenko beam with solid (rectangular) cross-section is investigated. Only proportional feedback control law is implemented in this study. To perform to have a good understanding of piezoelectric effects. The model used here is relatively simple to thin-walled composite beam theory.

Figure 4.1 shows the laminated beam considered in this case. The piezoelectric layers are located continuously at the top and the bottom of the beam. Two different composite configurations, symmetric and non-symmetric, are considered and their lamination system can be seen in Figure 4.2 and geometric and material properties can be found in Table 4.1

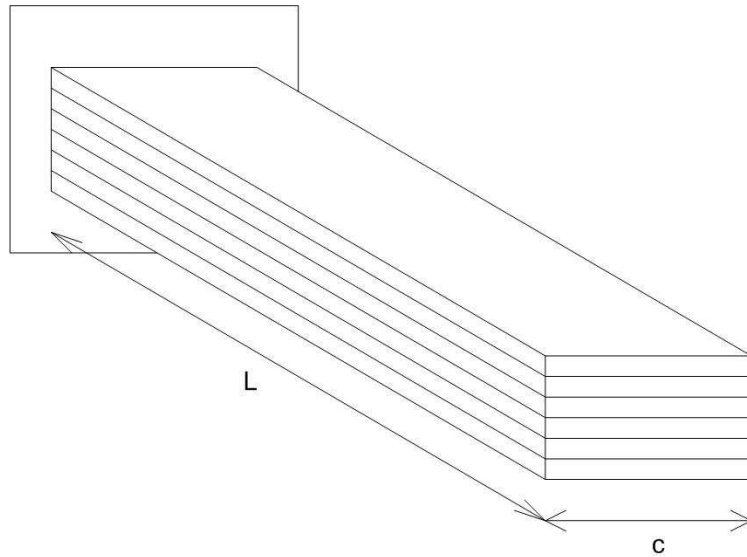


Figure 4.1: Timoshenko laminated beam

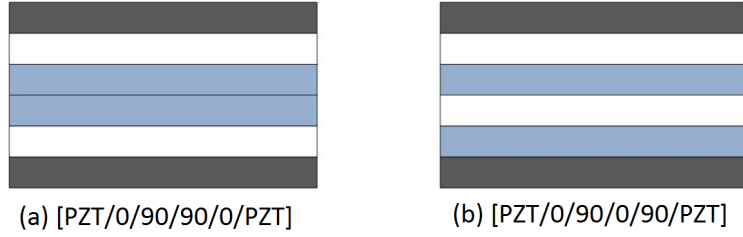


Figure 4.2: (a) Symmetric laminate, (b) Non-symmetric laminate

The governing equations of motion are given for most general piezo-laminated beam as follows. One should see Ref. [21–23] for more detailed formulation and discussion.

$$\frac{\partial}{\partial x} \left(A_{11} \frac{\partial U_0}{\partial x} + B_{11} \frac{\partial \phi}{\partial x} + \bar{E}_{11} \right) = \frac{\partial}{\partial t} [(I_1 \dot{U}_0) + (I_2 \dot{\phi})] \quad (4.46)$$

$$\frac{\partial}{\partial x} \left(A_{55} \left(\phi + \frac{\partial W}{\partial x} \right) - P \frac{\partial W}{\partial x} \right) = \frac{\partial}{\partial t} [(I_1 \dot{W})] + q \quad (4.47)$$

$$\frac{\partial}{\partial x} \left(B_{11} \frac{\partial U_0}{\partial x} + D_{11} \frac{\partial \phi}{\partial x} + F_{11} \right) - A_{55} \left(\phi + \frac{\partial W}{\partial x} \right) = \frac{\partial}{\partial t} [(I_3 \dot{\phi}) + (I_2 \dot{U}_0)] \quad (4.48)$$

where mass related terms are

$$(I_1, I_2, I_3) = c \int_{-h/2}^{h/2} \rho(1, z, z^2) dz \quad (4.49)$$

ρ , q and P denote mass density of each layer, transverse distributed load and axial compressive force, respectively. Also, the superscript $(\dot{})$ stands for time derivative. Moreover, \bar{E}_{11} and F_{11} denote induced axial force and induced bending moment, respectively. It is also given as, $F_{11} = G \bar{f} \phi'(x, t)$ and G is proportional feedback gain.

Table 4.1: Material Properties and Geometric Dimensions of Timoshenko Beam

	Graphite-Epoxy	PZT-5H		Graphite-Epoxy	PZT-5H
E_1	144.8 GPa	6.3 GPa	h	$1.27 \cdot 10^{-4}$ m	$2 \cdot 10^{-4}$
E_2	9.65 GPa	6.3 GPa	L	0.254 m	0.254 m
G_{12}	7.1 GPa	24.8 GPa	c	0.0254 m	0.0254 m
G_{13}	7.1 GPa	-	Q_{11}	145.7 GPa	68.36 GPa
G_{23}	5.92 GPa	-	Q_{22}	9.708 GPa	68.36 GPa
ν_{12}	0.3	0.28	Q_{12}	2.878 GPa	16.26 GPa
$\bar{\epsilon}$	-	$1.593 \cdot 10^{-8}$	Q_{66}	7.1 GPa	0
d_{31}	-	$-166 \cdot 10^{-12}$	ρ	1560 kg/m ³	7600 kg/m ³

The boundary conditions,

$$N_x = A_{11} \frac{\partial U_0}{\partial x} + B_{11} \frac{\partial \phi}{\partial x} + \bar{E}_{11} = P; \quad U_0 = 0 \quad (4.50)$$

$$Q_{xz} = A_{55} \left(\phi + \frac{\partial W}{\partial x} \right) - P \frac{\partial W}{\partial x} = 0; \quad W = 0 \quad (4.51)$$

$$M_x = B_{11} \frac{\partial U_0}{\partial x} + D_{11} \frac{\partial \phi}{\partial x} + F_{11} = 0; \quad \phi = 0 \quad (4.52)$$

For free vibration case, all external loads vanish, $q = 0$ and $P = 0$. Also, induced axial force \bar{E}_{11} is zero due to equality in opposite direction. The general solution

$$U_0(x, t) = u_0(x) e^{i\omega t} \quad (4.53)$$

$$W(x, t) = w(x) e^{i\omega t} \quad (4.54)$$

$$\phi(x, t) = \phi(x) e^{i\omega t} \quad (4.55)$$

Then, the equations of motion become

$$A_{11} u_0'' + B_{11} \phi'' = -\omega^2 I_1 u_0 - \omega^2 I_2 \phi \quad (4.56)$$

$$A_{55} \phi' + A_{55} w'' = -\omega^2 I_1 w \quad (4.57)$$

$$\left(B_{11} + \frac{G\bar{f}}{h_0} \right) u_0'' + (D_{11} + G\bar{f}) \phi'' - A_{55} (\phi + w') = -\omega^2 I_3 \phi - \omega^2 I_2 u_0 \quad (4.58)$$

4.4.1.1 Symmetric case

The cross-ply symmetric laminate has six layers and the configuration of $[PZT/0^\circ/90^\circ/90^\circ/0^\circ/PZT]$. Symmetric configuration simplifies the equations of motion due to $B_{11} = 0$ and $I_2 = 0$

$$A_{11} u_0'' + \omega^2 I_1 u_0 = 0 \quad (4.59)$$

$$A_{55} \phi' + A_{55} w'' = -\omega^2 I_1 w \quad (4.60)$$

$$(D_{11} + G\bar{f}) \phi'' - A_{55} (\phi + w') = -\omega^2 I_3 \phi \quad (4.61)$$

The boundary conditions

$$A_{11}u'_0 = 0; \quad u_0 = 0 \quad (4.62)$$

$$A_{55}(\phi + w') = 0; \quad w = 0 \quad (4.63)$$

$$(D_{11} + G\bar{f})\phi' = 0; \quad \phi = 0 \quad (4.64)$$

The results are obtained by both analytically and Extended-Galerkin Method for first three modes. The natural frequencies are tabulated in Table 4.2, 4.3 and 4.4 given as

Table 4.2: Comparison of First Natural Frequencies for Timoshenko Beam

Feedback Gain G	ω_1 (rad/s) Ref. [21]	ω_1 (rad/s) Analytic	ω_1 (rad/s) EGM	ω_1 (rad/s) DTM
0	9.78	9.83	9.83	9.83
5	10.74	10.80	10.79	10.78
15	12.33	12.50	12.50	12.50
24.3	13.76	13.90	13.90	13.90

Table 4.3: Comparison of Second Natural Frequencies for Timoshenko Beam

Feedback Gain G	ω_2 (rad/s) Ref. [21]	ω_2 (rad/s) Analytic	ω_2 (rad/s) EGM	ω_2 (rad/s) DTM
0	61.11	61.61	61.61	61.61
5	67.16	67.65	67.65	67.65
15	77.66	78.35	78.35	78.35
24.3	86.42	87.13	87.13	87.13

Table 4.4: Comparison of Third Natural Frequencies for Timoshenko Beam

Feedback Gain G	ω_3 (rad/s) Ref. [21]	ω_3 (rad/s) Analytic	ω_3 (rad/s) EGM	ω_3 (rad/s) DTM
0	171.17	172.50	172.55	172.50
5	187.88	189.42	189.18	189.42
15	217.49	219.38	219.28	219.38
24.3	241.84	243.95	243.91	243.96

4.4.1.2 Non-Symmetric case

The solution for non-symmetric case does not contain any simplification due to configuration unlike symmetric case. In order to solve the system analytically, three equations of motion must be decoupled first. One should see Ref. [21] to obtain a detailed explanation about analytic solution. As a result, obtained results are given in Table 4.5, 4.6 and 4.7 below.

Table 4.5: Comparison of First Natural Frequencies for Timoshenko Beam

Feedback Gain G	ω_1 (rad/s) Ref. [21]	ω_1 (rad/s) Analytic	ω_1 (rad/s) EGM	ω_1 (rad/s) DTM
0	9.1	9.18	9.24	9.181
5	10.22	10.114	10.26	10.116
15	12.13	11.764	12.05	11.765
21.55	13.24	12.732	13.08	12.729

Table 4.6: Comparison of Second Natural Frequencies for Timoshenko Beam

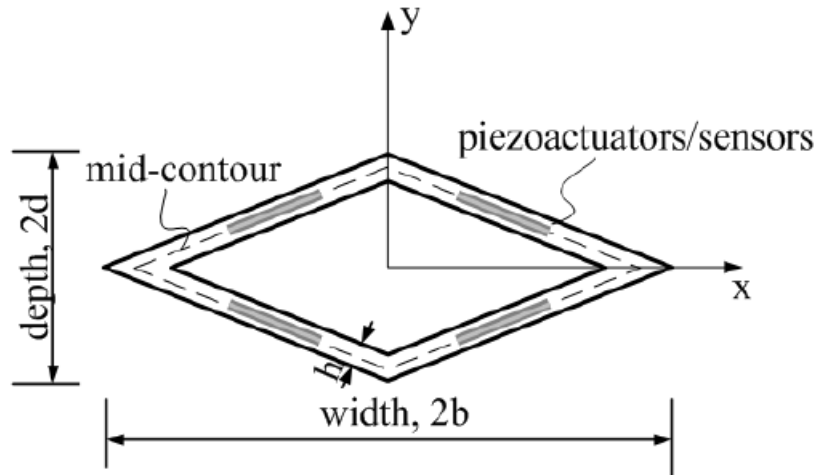
Feedback Gain G	ω_2 (rad/s) Ref. [21]	ω_2 (rad/s) Analytic	ω_2 (rad/s) EGM	ω_2 (rad/s) DTM
0	57.08	57.52	57.93	57.517
5	64.02	63.368	64.32	63.368
15	76	73.685	75.49	73.685
21.55	82.93	79.578	81.99	79.72

Table 4.7: Comparison of Third Natural Frequencies for Timoshenko Beam

Feedback Gain G	ω_3 (rad/s) Ref. [21]	ω_3 (rad/s) Analytic	ω_3 (rad/s) EGM	ω_3 (rad/s) DTM
0	159.8	160.96	162.22	160.957
5	179.2	177.31	180.08	177.31
15	212.75	206.128	211.13	206.128
21.55	232.11	230.775	229.57	222.97

4.4.2 Thin-walled Composite Beam

The equations of motion are solved for free vibration case with proportional and velocity feedback control laws separately. The effects of piezoelectric layers are included to mass and stiffness matrices where they are neglected in most studies. Embedded piezoelectric layers and cross section of the beam are demonstrated in Fig 4.3. Also properties of the piezoelectric material, PZT-4, is given in Table 4.8

**Figure 4.3:** Variation of stiffness quantities with ply angle**Table 4.8:** Material Properties of Piezoelectric Layers

PZT-4	
$C_{11} = C_{22}$	139 GPa
C_{12}	77.77 GPa
C_{13}	74.30 GPa
C_{33}	115 GPa
C_{44}	25.59 GPa
ρ_p	7498 kg/m ³
e_{31}	-5.202 N/Vm
e_{33}	15.101 N/Vm

Figure 4.4 demonstrates the variation of stiffness quantities with respect to ply angles. Since the width and the depth of the beam are equal, the transverse and lateral stiffness quantities correspond to bending and shear have the same value, respectively. Besides, the bending stiffness quantities are dominant when compared to others. In the absence of feedback gain, another figure is plotted to show the variation of the first two natural frequencies with respect to ply angle (Figure 4.5). The natural frequencies of the first and second transverse bending modes are obtained to have the same values as the ones of lateral bending modes.

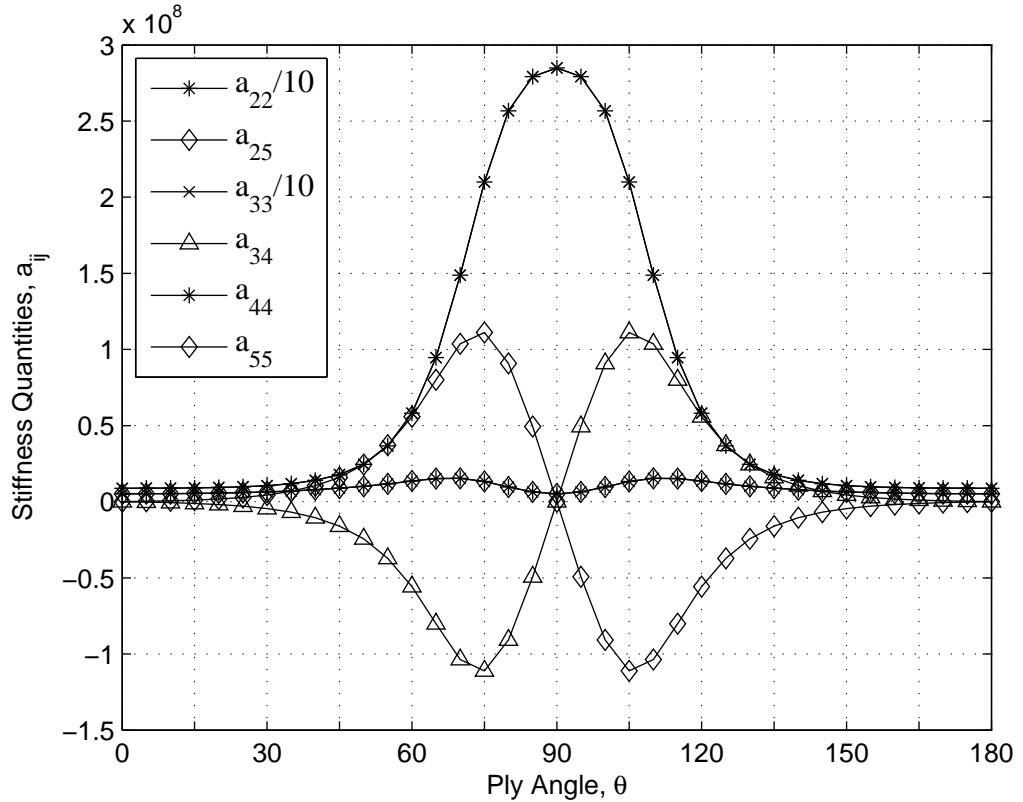


Figure 4.4: Variation of stiffness quantities with ply angle

This study utilizes two different control laws to achieve active vibration control of the structure. The first one is proportional feedback control and in this control law, actuated moment at the wing tip is proportional to the displacement at the wing tip, vertical or horizontal. The second one is velocity feedback control in which piezoelectrically induced moment at wing tip is proportional to the velocity at the wing tip, either flapwise or chordwise. As a result, the analyses with feedback gains are carried out and results are shown in several figures below.

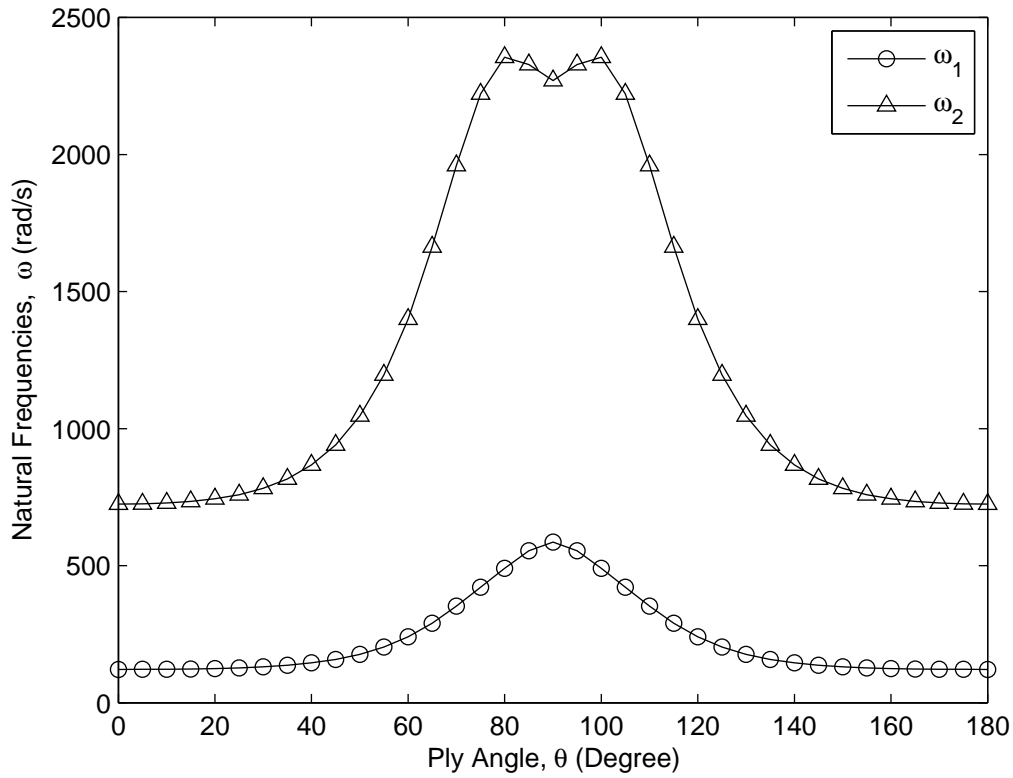


Figure 4.5: Natural frequencies of aircraft wing with diamond shaped cross section

Figure 4.6 shows the first natural frequencies versus proportional feedback control gain for different ply angles. In order to analyze the model better, some parameters are changed. Figure 4.7 provides information about first natural frequencies versus proportional feedback control gain for selected values of length and $\theta=0$. In Figure 4.8, relation between first natural frequencies and proportional feedback control gain for selected slenderness ratios and $\theta=0$, while keeping depth constant.

Figure 4.9 shows the implementation of velocity feedback control. This figure provides information about first natural frequencies for selected ply angles and how they vary with velocity feedback control gain. Similar to Figure 4.7, Figure 4.10 provides information about first natural frequencies versus velocity feedback control gain for selected values of length and $\theta=0$.

As mentioned before, in the absence of velocity feedback control it is obvious that there is no damping on structural model. In Figure 4.11, damping factor is shown versus velocity feedback control gain. All obtained results show an agreement with results provided in Ref. [9].

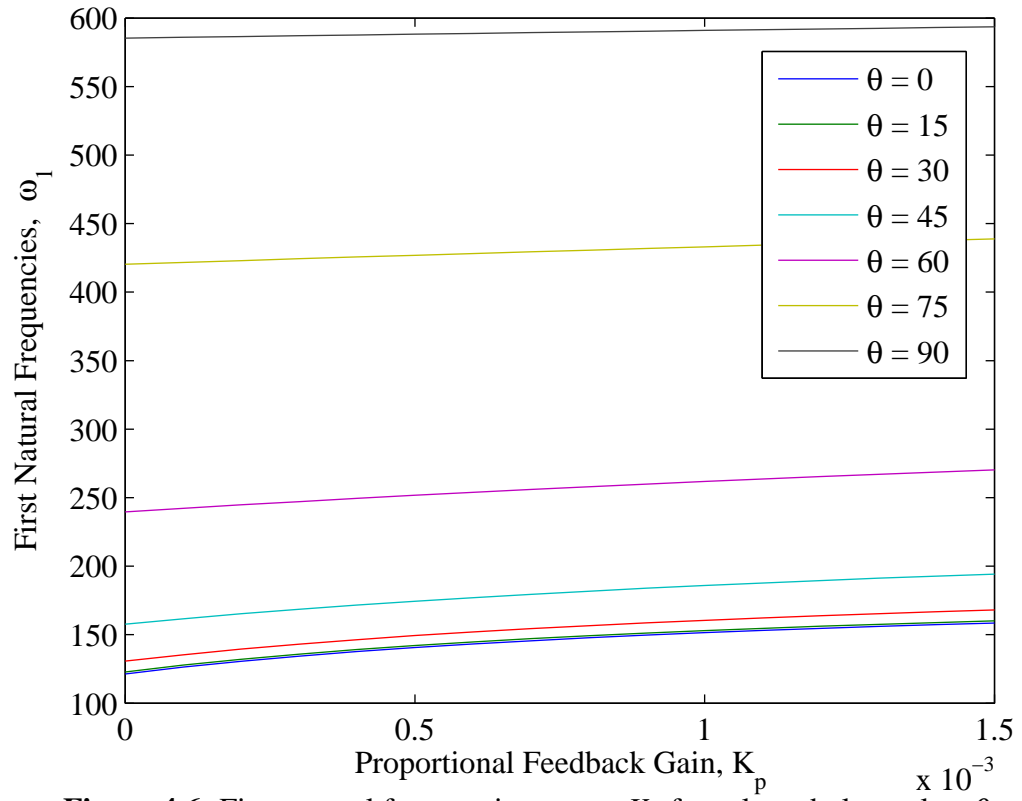


Figure 4.6: First natural frequencies versus K_p for selected ply angles, θ

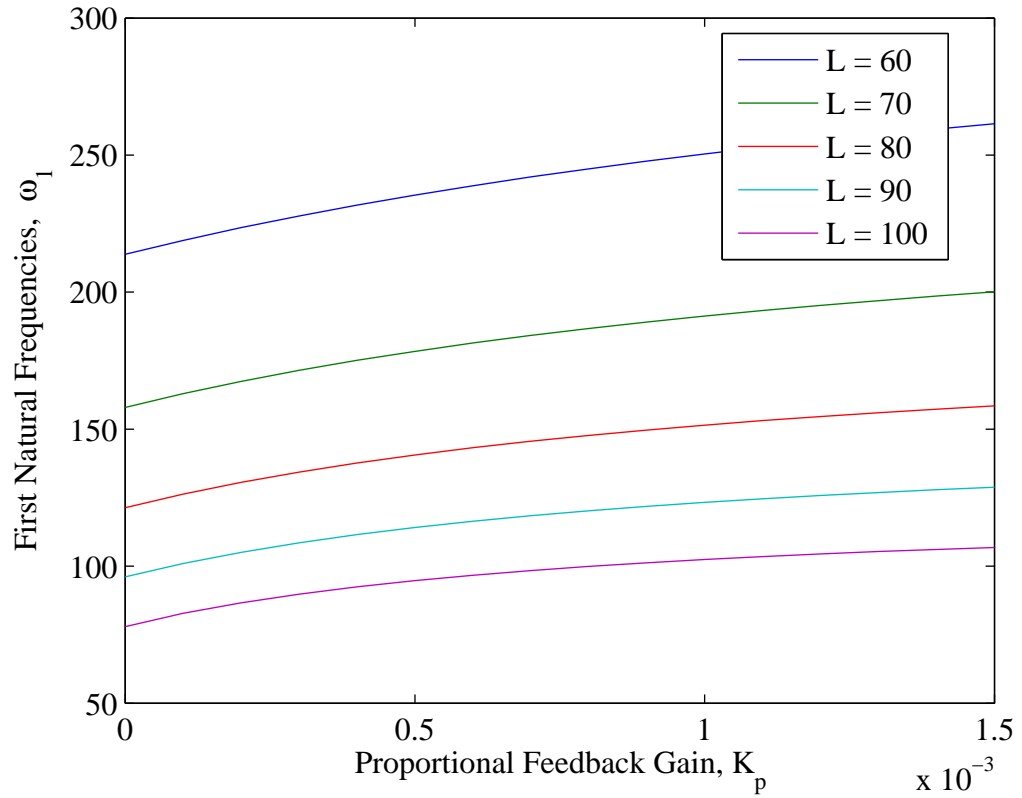


Figure 4.7: First natural frequencies versus K_p for selected values of length, L

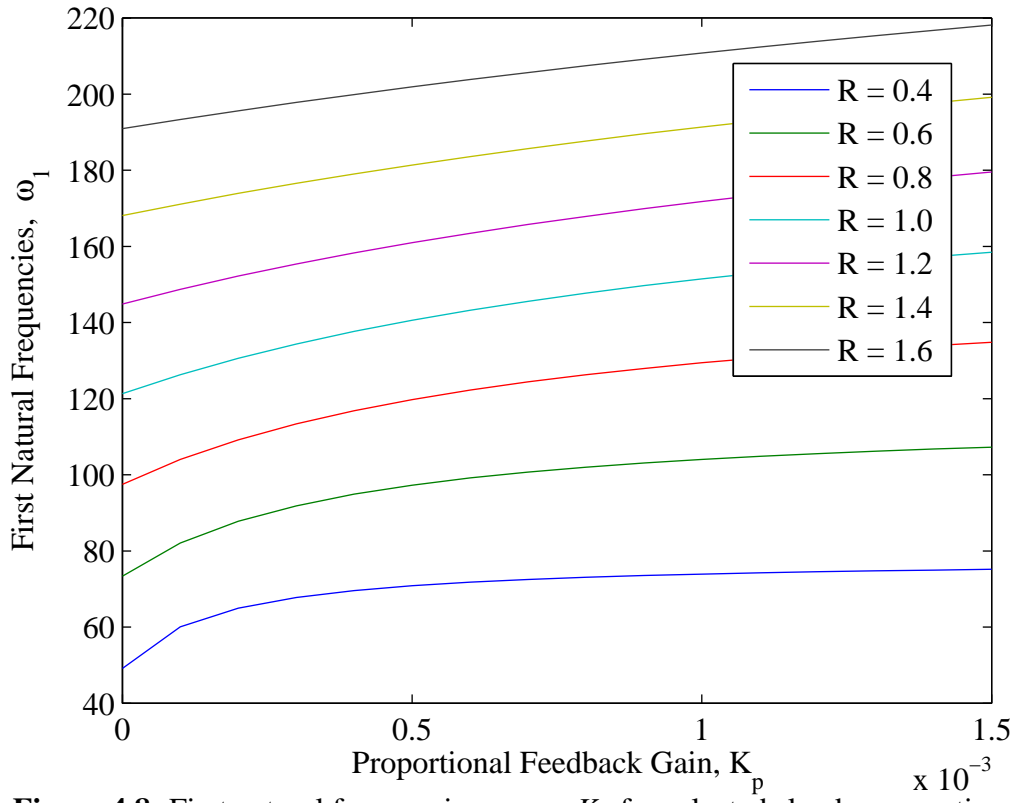


Figure 4.8: First natural frequencies versus K_p for selected slenderness ratios, R

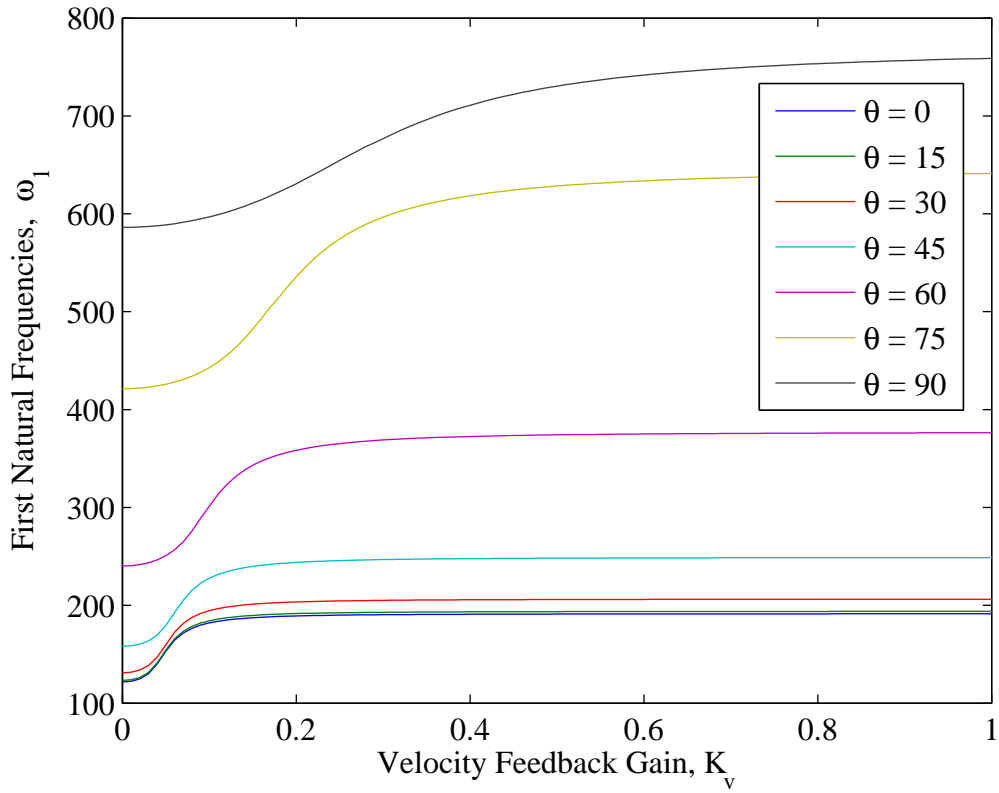


Figure 4.9: First natural frequencies versus K_v for selected ply angles, θ

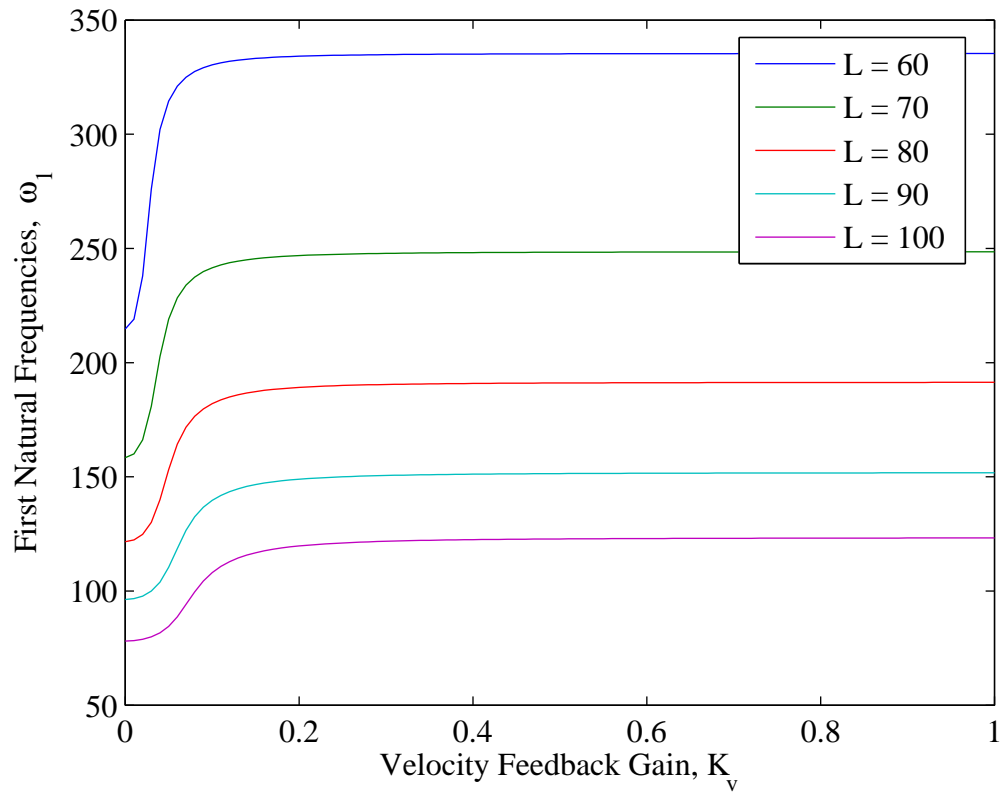


Figure 4.10: First natural frequencies versus K_v for selected values of length, L

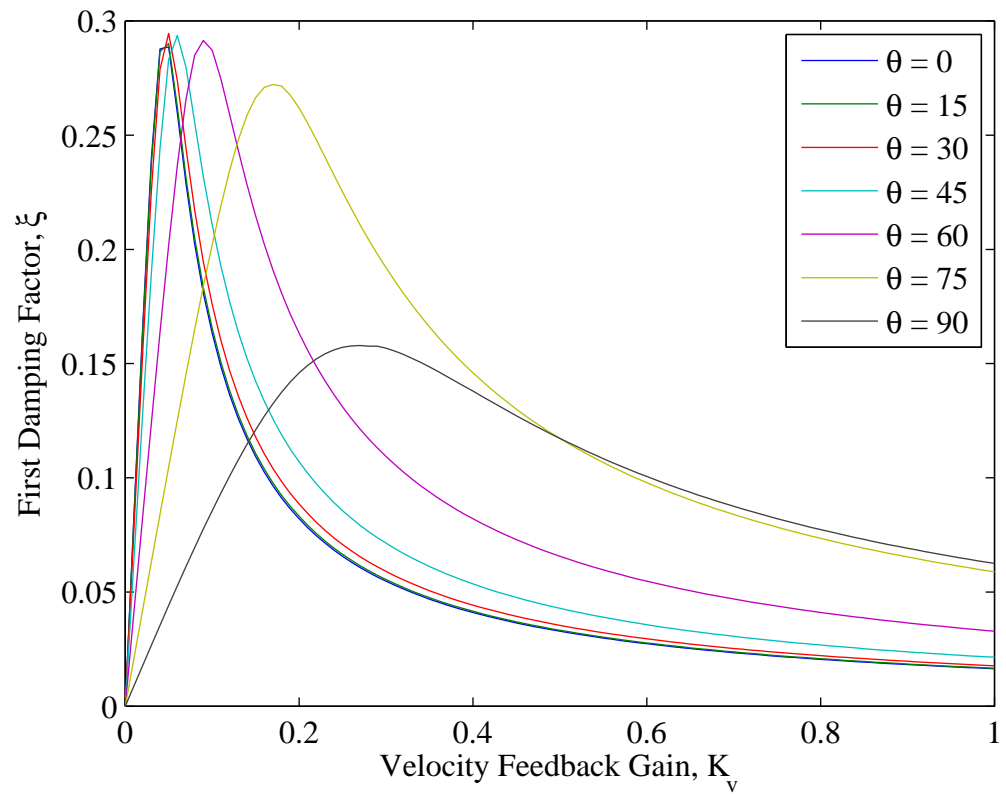


Figure 4.11: First damping factors versus K_v for selected ply angles, θ

4.5 Optimal Feedback Control Law

In this section another control method is implemented and dynamic response of the beam is investigated. This new control method is called optimal control and utilizes a mathematical optimization in order to minimize a certain cost function. The aim is to drive the final value of the state $\mathbf{x}(t)$ to a desired value in an arbitrary short time with a control input of $\mathbf{u}(t)$ Ref. [24] This control is based on a linear quadratic controller design. As a result, equations of motion under influence of control input are expressed as

$$\dot{\mathbf{x}}(t) = \mathbf{A}\mathbf{x}(t) + \mathbf{W}\mathbf{u}(t) + \mathbf{B}\mathbf{Q}(t) \quad (4.65)$$

As stated above, $\mathbf{u}(t)$ is control input to be found. Besides, here

$$\mathbf{A} = \begin{bmatrix} \mathbf{0} & \mathbf{I} \\ -\mathbf{M}^{-1}\mathbf{K} & \mathbf{0} \end{bmatrix} \quad (4.66)$$

$$\mathbf{W} = \begin{bmatrix} \mathbf{0} \\ -\mathbf{M}^{-1}\mathbf{F} \end{bmatrix} \quad (4.67)$$

$$\mathbf{B} = \begin{bmatrix} \mathbf{0} \\ -\mathbf{M}^{-1} \end{bmatrix} \quad (4.68)$$

Besides, \mathbf{F} is the piezoactuator influence vector and defined as

$$\mathbf{F} = [\varphi'_i(z_2) - \varphi'_i(z_1)] \quad (4.69)$$

By minimizing the control effort and the response of the closed-loop system linear quadratic regulator (LQR) control algorithm is achieved. Two different situations should be mentioned here. The cost function can be defined in two separate ways. As the first case, external excitation is included in the cost function or performance index. As the second case, external excitation is not included in the performance index. In this study the second case is investigated. One should refer to Ref. [8] to obtain more knowledge on first case. Therefore, the cost function can be defined as

$$J = \frac{1}{2} \int_{t_0}^{t_f} (\mathbf{x}^T \mathbf{Z} \mathbf{x} + \mathbf{u}^T \mathbf{R} \mathbf{u}) dt \quad (4.70)$$

Here, \mathbf{Z} and \mathbf{R} are positive semidefinite the state weighting matrix and positive definite symmetric the control weighting matrix, respectively. t_0 and t_f stand for initial and final time.

The state weighting and the control weighting matrices are chosen to be balancing the needs; minimizing the control effort and dynamic response. Their expressions are given as below

$$\mathbf{Z} = \begin{bmatrix} \alpha \mathbf{K} & \mathbf{0} \\ \mathbf{0} & \beta \mathbf{M} \end{bmatrix} \quad (4.71)$$

$$\mathbf{R} = \eta \mathbf{F}^T \mathbf{K}^{-1} \mathbf{F} \quad (4.72)$$

where η stands for scale factor. α and β are named as weighting coefficients and restrictions on them are $\alpha\beta \geq 0$ and $\alpha + \beta > 0$. Under the circumstances \mathbf{Z} is an indication of the total energy of the system as kinetic and potential

$$\frac{1}{2} \int_{t_0}^{t_f} \mathbf{x}^T \mathbf{Z} \mathbf{x} dt = \frac{1}{2} \int_{t_0}^{t_f} [\dot{\mathbf{q}}^T \beta \mathbf{M} \dot{\mathbf{q}} + \mathbf{q}^T \alpha \mathbf{K} \mathbf{q}] dt \quad (4.73)$$

Regarding to all the information at hand, the steady-state Riccati equation is

$$\mathbf{Z} + \mathbf{P} \hat{\mathbf{A}} + \hat{\mathbf{A}}^T \mathbf{P} - \mathbf{P} \mathbf{W} \mathbf{R}^{-1} \mathbf{W}^T \mathbf{P} = 0 \quad (4.74)$$

\mathbf{P} is the positive definite solution to the steady-state Riccati equation. Then, the optimal gain matrix can be obtained as

$$\mathbf{G} = \mathbf{R}^{-1} \mathbf{W}^T \mathbf{P} \quad (4.75)$$

As a result, with optimal feedback control law, control input is written as

$$\mathbf{u}(t) = -\mathbf{G}\mathbf{x}(t) \quad (4.76)$$

4.6 Dynamic Response

In this section, the dynamic response of the thin-walled composite beam under different control laws is investigated. The comparisons are held between control laws.

Concerning solution methodology, since there are very large number of equations, the modal analysis is utilized here to making solution rather easy and reduce computation time. This method is highly recommended due to its uncoupling feature. The modal analysis method depends on the vector of eigenvectors and mode amplitudes. In this technique physical coordinates are turned into modal or generalized coordinates using eigenvalues and eigenvectors. These new coordinates are also referred as principal coordinates. Therefore the state vector can be rewritten as

$$\mathbf{X}(t) = \Phi \xi(t) \quad (4.77)$$

Here Φ represents modal matrix while ξ is the modal coordinates vector. On the other hand, force terms should also be generalized

$$\mathbf{f}(t) = \Phi^T \mathbf{Q}(t) \quad (4.78)$$

As a result equations of motion can be written in terms of generalized coordinates

$$\Phi^T \mathbf{M} \Phi \ddot{\xi}_s(t) + \Phi^T \mathbf{C} \Phi \dot{\xi}_s(t) + \Phi^T \mathbf{K} \Phi \xi_s(t) = \Phi^T \mathbf{Q}(t) \quad (4.79)$$

Then the discretized displacements can be rearranged as Ref. [7]

$$u_0(z, t) = N_u^T(z) \Phi_u \xi_s(t) \quad (4.80)$$

$$v_0(z, t) = N_v^T(z) \Phi_v \xi_s(t) \quad (4.81)$$

$$\theta_x(z, t) = N_x^T(z) \Phi_x \xi_s(t) \quad (4.82)$$

$$\theta_y(z, t) = N_y^T(z) \Phi_y \xi_s(t) \quad (4.83)$$

Here, $\Phi_u, \Phi_v, \Phi_x, \Phi_y$ are $N \times m$ eigenvector matrices while m is the number of modes taken into account. In this study six modes are considered.

Then all the matrices in Eq. 4.37 and 4.65 can be cast into generalized form. The problem in modal analysis technique here, in most cases, the damping matrix does not become a diagonal matrix resulting no decoupling. Three possible solutions are suggested for this situation and they can be listed as

- Diagonalization
- Complex Eigensystem
- Direct Time Integration, DTI

In diagonalization technique, if damping is light, damping matrix can be diagonalized by using undamped frequencies and mode shapes. However, diagonalization cannot properly model damping effects of some situations accurately Ref. [26]. They are

- Structures with local damper devices
- Structure-media interaction
- Active control systems

In this study, investigated problem lies in the three scenarios listed above. Therefore, diagonalization is not an adequate solution method for the problem at hand.

The complex eigensystem method is an exact solution methodology, and requires no approximation. The damping strength does not change anything. The only problem is for a large number of degrees of freedom, solution may be time consuming. Also expertise in math and engineering is required. In this study this solution type is preferred.

Direct time integration is another method for solving such systems. Besides, It has the feature of solving nonlinear equations of motion different from the other methods introduced. Additionally, it does not involve with coordinate transformation or complex arithmetic.

The complex eigensystem is employed to solve the equations of motion. The dynamic response of the beam is obtained under a unit impulse at beam tip. Obtained results under different control law types are plotted below in Fig. 4.12 and 4.13.

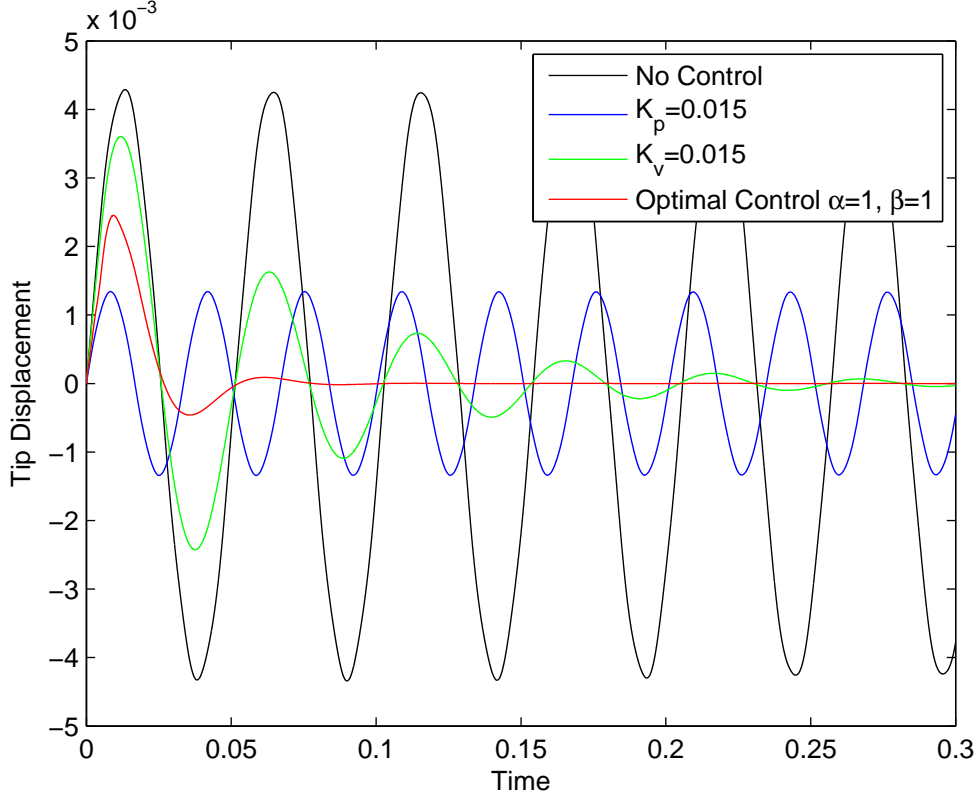


Figure 4.12: Comparison of different control laws under applied Dirac Delta

The figure above, Fig. 4.12, is the most significant figure obtained in this study. It clearly expresses the distinction between the implemented control laws. As expected, in the absence of any control method, dynamic response is obtained harmonically. Implementation of proportional feedback control reduces the amplitude but does not change the dynamic characteristics of oscillation, briefly, response remains harmonic. It was stated in previous chapters, application of velocity feedback control generates damping to the system and can be tracked with the green line. The damping of oscillation under applied velocity feedback gain can clearly be seen in the figure. Lastly, red line represents the optimal control law for selected α and β values. Optimal control was defined as a control law that minimizes the cost function which was determined to consist of the control effort and the response of closed-loop system.

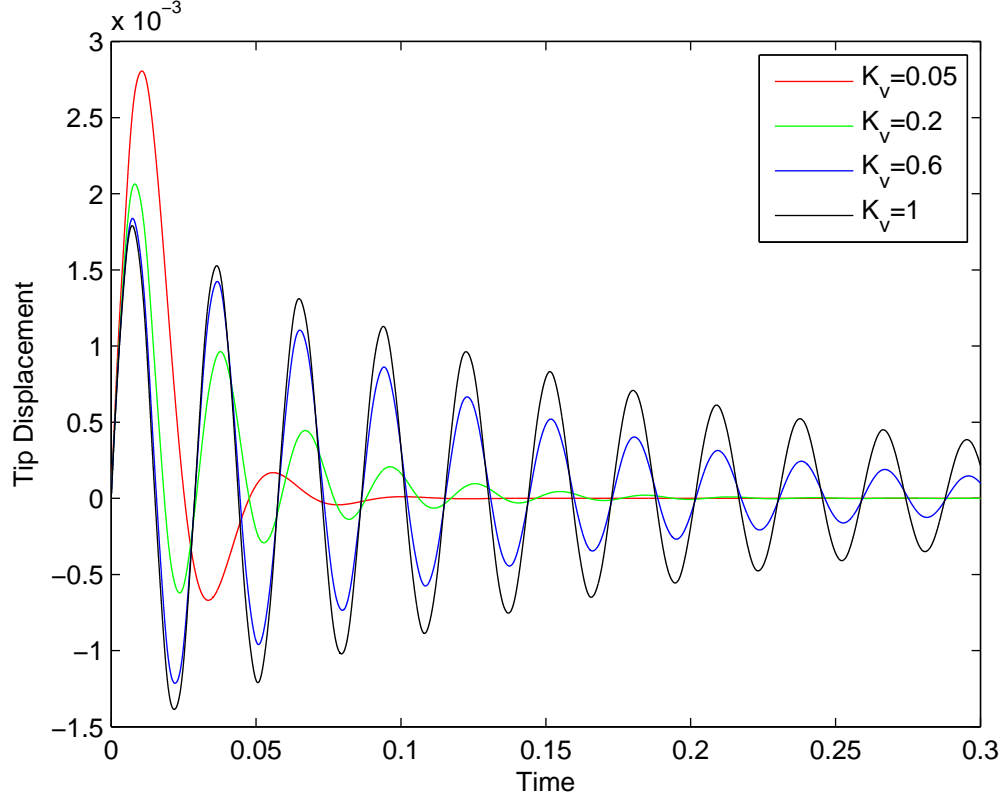


Figure 4.13: Comparison of different values of velocity feedback gains

In Fig. 4.13, the dynamic response of the beam under unit impulse, is compared for different values of velocity feedback gain. Considering this figure, it is seen that for the value of $K_v = 0.05$ the beam has the maximum damping effect and as K_v increases the damping effect reduces. Actually, this is a predicted result from the Fig. 4.11 which has the maximum damping ratio at around the value of $K_v = 0.05$. About the amplitudes, as the velocity feedback gain increases, natural frequencies which is an indication of stiffness level of the beam gets higher, see Fig. 4.9, yielding to lower amplitudes.

In Fig. 4.14, under different control parameters of α and β , optimal control feedback law is investigated. It was tried to make a logical statement for the parameters of α and β . As moving from left to right side in rows, values of α parameter increase and as moving from top to bottom in columns, values of β parameter increase. Some constant values which are 0, 0.1, 1, 10 and 100 are assigned to them.

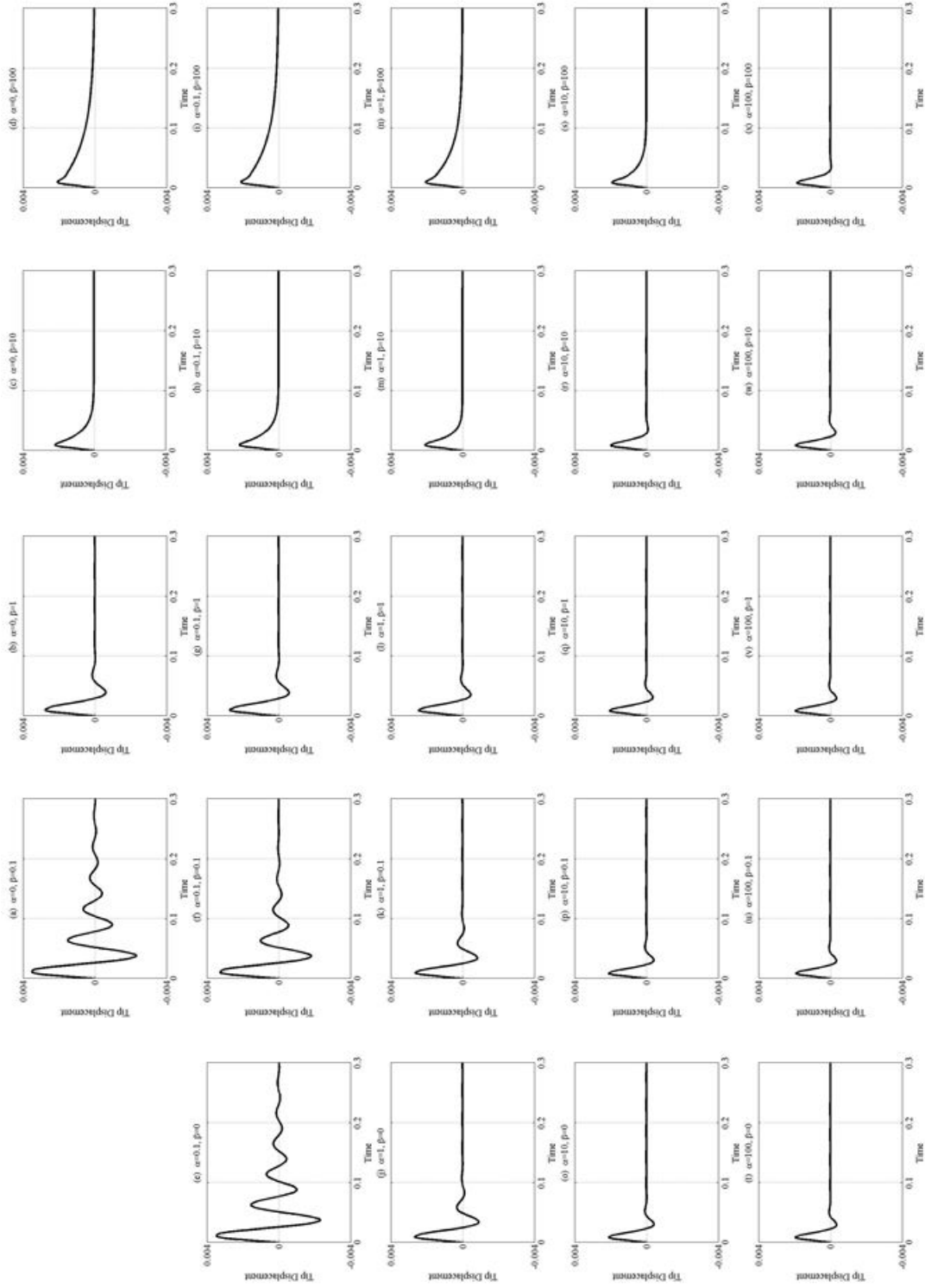


Figure 4.14: Dynamic response of the beam for optimal control under various control parameters

It is seen from the figure that as α increases, amplitudes decrease. Therefore, it is realized that α is an indication of and highly related to amplitudes. On the other hand, as β increases, the time that oscillations completely damped and number of peaks decrease. It yields to a result that damping time is a function of parameter β . One thing to notice is that as β is increased to 100 from 10 damping time increases. This situation can be explained as, the system changes to overdamped phase from critically damped phase or underdamped phase. The critically damped phase occurs at value of around 10, and then when β increases it transforms into overdamped phase. The illustration for that phenomena is given in the following figure.

As can be seen from Fig. 4.15, as damping ratio increases dynamic response changes and damping time decreases. Maximum damping time occurs at undamped case and minimum appears on critically damped case. However, when damping ratio increases beyond critical level, overdamped case occurs and damping time increases.

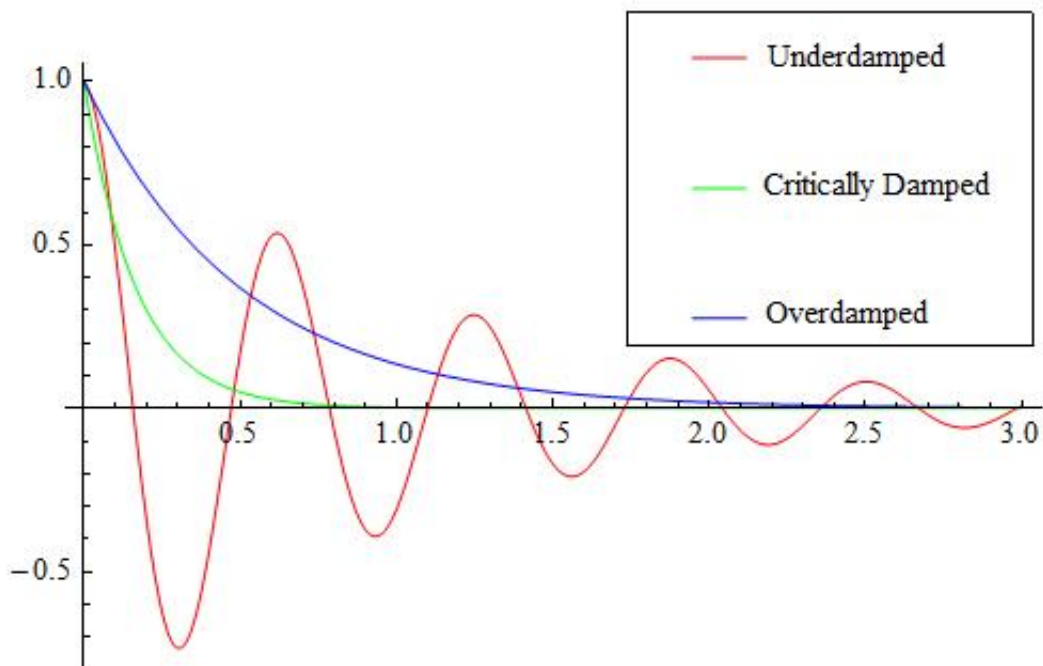


Figure 4.15: Different damping characteristics

5. CONCLUSION

In conclusion, dynamic analyses are performed for aircraft wings modelled as thin-walled composite beams and active vibration control is achieved using piezoelectric actuation. Depending on the implemented control law, dynamic behaviours and natural frequencies of the beam is controlled in a predictable manner.

First, theory of thin-walled composite beams is explained and structural modelling is stated profoundly for a cantilever beam. The governing equations of motion of the beam are derived and a rectangular-box cross-section is used. The natural frequencies are obtained for box-beam and results are compared to the ones provided by previous studies.

Prior to implementation of active control mechanism, the beam is modelled as diamond shaped thin-walled beam and dynamic analyses are conducted. Variation of natural frequencies and stiffness quantities versus ply angles are depicted.

Secondly, active vibration control is applied to the aircraft wings. In order to acquire a good understanding about piezoelectricity and its application on structures, initially a rectangular laminated beam is considered. Appropriate voltages are applied to piezoelectric layers located at top and bottom of the beam. As a result, induced moments and forces are obtained and their influence on natural frequencies are investigated.

Afterwards, active vibration control is used in thin-walled composite diamond shaped beams with two different closed loop control laws. The piezoelectric layers are embedded into the host structure and they shift mass and stiffness matrices, resulting a change in natural frequencies, even in the absence of applied gain. Proportional and velocity feedback control laws are applied separately and their influences are investigated in each case. The study revealed that velocity feedback control is more sensitive than proportional one. Also, optimal control law is implemented on the system and dynamic response of the beam is obtained. The dynamic response

is examined under different control laws and comparison is made for Dirac Delta impulse.

As future work, it is planned to extend the study to be applicable to much more complex structures, like tapered aircraft wings. Also acceleration feedback control law is intended to be applied. Ultimately, behaviour of the structure under external forces will be also investigated and control will be achieved.

REFERENCES

- [1] **Librescu, L. and Ohseop, S.** (2006). *Thin-walled composite beams: Theory and Application*, Springer, The Netherlands.
- [2] **Berdichevsky, V., Armanios, E. and Badir, A.** (1992). Theory of anisotropic thin-walled closed-cross-section beams, *Composites Engineering*, **2**(5-7), 411-432.
- [3] **Rehfield, L.W., Atilgan, A.R. and Hodges, D.H.** (1990). Nonclassical Behavior of Thin-Walled Composite Beams with Closed Cross Sections, *Journal of the American Helicopter Society*, **35**(2), 42–50.
- [4] **Dancila, D.S. and Armanios, E.A.** (1998). The influence of coupling on the free vibration of anisotropic thin-walled closed-section beams, *International Journal of Solids and Structures*, **35**(23), 3105 – 3119.
- [5] **Song, O. and Librescu, L.**(1993). Free Vibration of Anisotropic Composite Thin-Walled Beams of Closed Cross-Section Contour, *Journal of Sound and Vibration*, **167**(1), 129-147.
- [6] **Tzou, H.S.** (1993). *Piezoelectric Shells, Distributed Sensing and Control of Continua*, Kluwer Academic Publication, Dordrecht.
- [7] **Qin, Z.** (2001). Vibration and Aeroelasticity of Advanced Aircraft Wings Modeled as Thin-Walled Beams –Dynamics, Stability and Control, *Ph.D. thesis*, VT, Blacksburg, VA
- [8] **Na, S.S.** (1997). Control of Dynamic Response of Thin-Walled Composite Beams using Structural Tailoring and Piezoelectric Actuation, *Ph.D. thesis*, VT, Blacksburg, VA
- [9] **Song, O., Kim, J-B. and Librescu, L.**(2001). Synergistic Implications of Tailoring and Adaptive Materials Technology on Vibration Control of Anisotropic Thin-Walled Beams, *International Journal of Engineering Science*, **39**(1), 71-94.
- [10] **Librescu, L., Meirovitch, L. and Na, S.S.**(1997). Control of Cantilever Vibration via Structural Tailoring and Adaptive Materials, *AIAA Journal*, **35**(8), 1309-1315.
- [11] **Librescu, L., Song, O. and Rogers, C.A.**(1993). Adaptive Vibrational Behavior of Cantilevered Structures Modelled as Composite Thin-Walled Beams, *International Journal of Engineering Science*, **31**(5), 775-792.

- [12] **Librescu, L. and Na, S.S.** (1996). Integrated Structural Tailoring and Control Using Adaptive Materials for Advanced Aircraft Wings, *Journal of Aircraft*, **33**(1), 203-213.
- [13] **Na, S.S. and Librescu, L.**(1998). Oscillation Control of Cantilevers via Smart Materials Technology and Optimal Feedback Control: Actuator Location and Power Consumption Issues, *International Journal of Engineering Science*, **7**(6), 833-842.
- [14] **Yildız, K., Eken, S. and Kaya, M.O.,** (2014), Active Vibration Control of Aircraft Wings Modeled as Thin Walled Composite Beams Using Piezoelectric Actuation , *ASME-IMECE, International Mechanical Engineering Congress and Exposition*, Montreal, QC, Canada, November 14-20.
- [15] **Durmaz, S.** (2013). Nonlinear Dynamic and Aeroelastic Analyses of Aircraft Wings, *Ph.D. thesis*, ITU, Istanbul, TURKEY.
- [16] **Nettles, A.T.** (1994). *Basic Mechanics of Laminated Composite Plates*, NASA Reference Publication 1351, MSFC, Alabama.
- [17] **Meirovitch, L.** (1997). *Principles and Techniques of Vibrations*, Prentice-Hall.
- [18] **Lagnese, J.E.** (1989). *Boundary Stabilization of Thin Plates*, SIAM Studies in Applied Mechanics, SIAM, Philadelphia, PA.
- [19] **Librescu, L. and Na, S.S.**(1998). Bending Vibration Control of Cantilevers Via Boundary Moment and Combined Feedback Control Law, *Journal of Vibration and Controls*, **4**(6), 733-746.
- [20] **Inman, D.J.** (2001). Active modal control for smart structures, *Phil. Trans. R. Soc. London, A*, **359**, 205-209.
- [21] **Fridman, Y. and Abramovich, H.**(2007). Enhanced structural behavior of flexible laminated composite beams, *Composite Structures*, **82**, 140-154.
- [22] **Abramovich, H.** (1998). Deflection control of laminated composite beams with piezoceramic layers - closed form solutions, *Composite Structures*, **43**, 217-231.
- [23] **Timoshenko, S. and Goodier, J.N.** (1951). *The Theory of Elasticity*, McGraw Hill, New York
- [24] **Na, S.S. and Librescu, L.** (2000). Optimal Vibration Control of Thin-Walled Anisotropic Cantilevers Exposed to Blast Loadings, *Journal of Guidance, Control and Dynamics*, **23**(3), 491-500.
- [25] **Hodges, Dewey H. and Pierce, G. Alvin** (2002). *Introduction to Structural Dynamics and Aeroelasticity*, Cambridge University Press, Cambridge.
- [26] **Felippa, C.** (2014). *Lecture on Introduction to Aerospace Structures Personal Collection of C. Felippa*, University of Colorado at Boulder, Colorado.

APPENDICES

APPENDIX A: Reduced Mass Terms and Stiffness Quantities

APPENDIX A: Reduced Mass Terms and Stiffness Quantities

Table A.1: The reduced mass terms, b_i .

$b_1 = \oint m_0 \mathrm{d}s$	$b_2 = \oint m_0 y \mathrm{d}s$
$b_3 = \oint m_0 x \mathrm{d}s$	$b_4 = \oint m_0 y^2 \mathrm{d}s$
$b_5 = \oint m_0 x^2 \mathrm{d}s$	$b_6 = \oint m_0 xy \mathrm{d}s$
$b_7 = \oint m_0 F_w \mathrm{d}s$	$b_8 = \oint m_0 y F_w \mathrm{d}s$
$b_9 = \oint m_0 x F_w \mathrm{d}s$	$b_{10} = \oint m_0 F_w^2 \mathrm{d}s$
$b_{11} = \oint m_0 \frac{\mathrm{d}x}{\mathrm{d}s} \mathrm{d}s$	$b_{12} = \oint m_0 \frac{\mathrm{d}y}{\mathrm{d}s} \mathrm{d}s$
$b_{13} = \oint m_2 \frac{\mathrm{d}x}{\mathrm{d}s} \frac{\mathrm{d}y}{\mathrm{d}s} \mathrm{d}s$	$b_{14} = \oint m_2 \left(\frac{\mathrm{d}x}{\mathrm{d}s} \right)^2 \mathrm{d}s$
$b_{15} = \oint m_2 \left(\frac{\mathrm{d}y}{\mathrm{d}s} \right)^2 \mathrm{d}s$	$b_{16} = \oint m_2 \left(\frac{\mathrm{d}x}{\mathrm{d}s} \right) r_t \mathrm{d}s$
$b_{17} = \oint m_2 \left(\frac{\mathrm{d}y}{\mathrm{d}s} \right) r_t \mathrm{d}s$	$b_{18} = \oint m_2 r_t^2 \mathrm{d}s$

Table A.2: Stiffness quantities, $a_{ij} = a_{ji}$. The acronyms E, CB, FB, CTS, FTS, W and T stand for Extensional, Chordwise Bending, Flapwise Bending, Chordwise Transverse Shear, Flapwise Transverse Shear, Warping and Twist, respectively.

Description	Coupling involved
$a_{11} = \oint K_{11} ds$	E
$a_{12} = \oint \left[K_{11}x + K_{14} \frac{dy}{ds} \right] ds$	E-CB
$a_{13} = \oint \left[K_{11}y - K_{14} \frac{dx}{ds} \right] ds$	E-FB
$a_{14} = \oint K_{12} \frac{dx}{ds} ds$	E-CTS
$a_{15} = \oint K_{12} \frac{dy}{ds} ds$	E-FTS
$a_{16} = \oint [K_{11}F_w - K_{14}r_t] ds$	E-W
$a_{17} = \oint K_{13} ds$	E-T
$a_{22} = \oint \left[K_{11}x^2 + 2K_{14}x \frac{dy}{ds} + K_{44} \left(\frac{dy}{ds} \right)^2 \right] ds$	CB
$a_{23} = \oint \left[K_{11}xy - K_{14}x \frac{dx}{ds} + K_{14}y \frac{dy}{ds} - K_{44} \frac{dx}{ds} \frac{dy}{ds} \right] ds$	CB-FB
$a_{24} = \oint \left[K_{12}x \frac{dx}{ds} + K_{24} \frac{dx}{ds} \frac{dy}{ds} \right] ds$	CB-CTS
$a_{25} = \oint \left[K_{12}x \frac{dy}{ds} + K_{24} \left(\frac{dy}{ds} \right)^2 \right] ds$	CB-FTS
$a_{26} = \oint \left[K_{11}F_w x - K_{14}r_t x + K_{14}F_w \frac{dy}{ds} - K_{44}r_t \frac{dy}{ds} \right] ds$	CB-W
$a_{27} = \oint \left[K_{13}x + K_{43} \frac{dy}{ds} \right] ds$	CB-T
$a_{33} = \oint \left[K_{11}y^2 - 2K_{14}y \frac{dx}{ds} + K_{44} \left(\frac{dx}{ds} \right)^2 \right] ds$	FB
$a_{34} = \oint \left[K_{12}y \frac{dx}{ds} - K_{24} \left(\frac{dx}{ds} \right)^2 \right] ds$	FB-CTS
$a_{35} = \oint \left[K_{12}y \frac{dy}{ds} - K_{24} \frac{dx}{ds} \frac{dy}{ds} \right] ds$	FB-FTS

$a_{36} = \oint \left[K_{11} F_w y - K_{14} r_t y - K_{14} F_w \frac{dx}{ds} + K_{44} r_t \frac{dx}{ds} \right] ds$	FB-W
$a_{37} = \oint \left[K_{13} y - K_{43} \frac{dx}{ds} \right] ds$	FB-T
<hr/>	
$a_{44} = \oint \left[K_{22} \left(\frac{dx}{ds} \right)^2 + \bar{K}_s \left(\frac{dy}{ds} \right)^2 \right] ds$	CTS
$a_{45} = \oint \left[K_{22} \frac{dx}{ds} \frac{dy}{ds} - \bar{K}_s \frac{dx}{ds} \frac{dy}{ds} \right] ds$	CTS-FTS
$a_{46} = \oint \left[K_{12} F_w \frac{dx}{ds} - K_{24} r_t \frac{dx}{ds} \right] ds$	CTS-W
$a_{47} = \oint \left[K_{23} \frac{dx}{ds} ds \right]$	CTS-T
<hr/>	
$a_{55} = \oint \left[\bar{K}_s \left(\frac{dx}{ds} \right)^2 + K_{22} \left(\frac{dy}{ds} \right)^2 \right] ds$	FTS
$a_{56} = \oint \left[K_{12} F_w \frac{dy}{ds} - K_{24} r_t \frac{dy}{ds} \right] ds$	FTS-W
$a_{57} = \oint \left[K_{23} \frac{dy}{ds} \right] ds$	FTS-T
<hr/>	
$a_{66} = \oint \left[K_{11} F_w^2 - 2K_{14} F_w r_t + K_{44} r_t^2 \right] ds$	W
$a_{67} = \oint \left[K_{13} F_w - K_{43} r_t \right] ds$	W-T
<hr/>	
$a_{77} = \oint \left[2K_{53} + K_{23} \psi \right] ds$	T
<hr/>	

The reduced elastic stiffness coefficients are defined as

$$\begin{aligned} Q_{ij} &= C_{ij} - C_{i3}C_{j3}/C_{33} & i, j &= 1, 2, 6 \\ Q_{kl} &= C_{kl} & k, l &= 4, 5 \end{aligned}$$

Modified stiffness quantities given in Eqs. ().

$$\begin{aligned} K_{11} &= A_{22} - \frac{A_{12}^2}{A_{11}} \\ K_{12} &= K_{21} = A_{26} - \frac{A_{12}A_{16}}{A_{11}} \\ K_{13} &= 2 \left(B_{26} - \frac{A_{12}B_{16}}{A_{11}} \right) + \psi \left(A_{26} - \frac{A_{12}A_{16}}{A_{11}} \right) \\ K_{14} &= K_{41} = B_{22} - \frac{A_{12}B_{12}}{A_{11}} \\ K_{22} &= A_{66} - \frac{A_{16}^2}{A_{11}} \\ K_{23} &= 2 \left(B_{66} - \frac{A_{16}B_{16}}{A_{11}} \right) + \psi \left(A_{66} - \frac{A_{16}^2}{A_{11}} \right) \\ K_{24} &= K_{42} = B_{26} - \frac{A_{16}B_{12}}{A_{11}} \\ K_{43} &= 2 \left(D_{26} - \frac{B_{12}B_{16}}{A_{11}} \right) + \psi \left(B_{26} - \frac{A_{16}B_{12}}{A_{11}} \right) \\ K_{44} &= D_{22} - \frac{B_{12}^2}{A_{11}} \\ K_{51} &= B_{26} - \frac{A_{12}B_{16}}{A_{11}} \\ K_{52} &= B_{66} - \frac{A_{16}B_{16}}{A_{11}} \\ K_{53} &= 2 \left(D_{66} - \frac{B_{16}^2}{A_{11}} \right) + \psi \left(B_{66} - \frac{A_{16}B_{16}}{A_{11}} \right) \\ K_{54} &= D_{26} - \frac{B_{12}B_{16}}{A_{11}} \end{aligned}$$

CURRICULUM VITAE

Name Surname: Kaan Yıldız

Place and Date of Birth: Beykoz, 02/11/1991

Address: Atatürk Mah. Alemdağ Cad. No:4/5 Ümraniye/İSTANBUL

E-Mail: yildizkaa@gmail.com

B.Sc.: Istanbul Technical University, Aeronautical Engineering, July 2013

List of Publications and Patents:

International Conference Publications:

- K.Yıldız, S. Eken, M. O. Kaya, Active Vibration Control of Aircraft Wings Modeled as Thin Walled Composite Beams Using Piezoelectric Actuation, ASME-International Mechanical Engineering Congress and Exposition, November 14-20, 2014, Montreal, QC, Canada.

National Conference Publications:

- K.Yıldız, S. Eken, M. O. Kaya, Piezoelektrik Malzemeler Yardımı ile Uçak Kanadının Aktif Titreşim Kontrolü, V. Ulusal Havacılık ve Uzay Konferansı, EÜ, Kayseri, 8-10 Eylül 2014.
- K.Yıldız, S. Eken, M. O. Kaya, Eksenel Uzama-Burulma Bağlaşımı Gösteren İnce Cidarlı Kompozit Kirişlerde Çarpılma Etkisinin İncelenmesi, V. Ulusal Havacılık ve Uzay Konferansı, EÜ, Kayseri, 8-10 Eylül 2014.

PUBLICATIONS/PRESENTATIONS ON THE THESIS

- K.Yıldız, S. Eken, M. O. Kaya, Active Vibration Control of Aircraft Wings Modeled as Thin Walled Composite Beams Using Piezoelectric Actuation, ASME-International Mechanical Engineering Congress and Exposition, November 14-20, 2014, Montreal, QC, Canada.